Development 140, 3826-3837 (2013) doi:10.1242/dev.095711

Dynamic analysis of *Arabidopsis* AP2 σ subunit reveals a key role in clathrin-mediated endocytosis and plant development

Lusheng Fan[1,2,*], Huaiqing Hao[1,*], Yiqun Xue[1,2], Liang Zhang[3], Kai Song[1,2], Zhaojun Ding[4], Miguel A. Botella[5], Haiyang Wang[6] and Jinxing Lin[1,‡]

SUMMARY

Clathrin-mediated endocytosis, which depends on the AP2 complex, plays an essential role in many cellular and developmental processes in mammalian cells. However, the function of the AP2 complex in plants remains largely unexplored. Here, we show in *Arabidopsis* that the AP2 σ subunit mutant (*ap2 σ*) displays various developmental defects that are similar to those of mutants defective in auxin transport and/or signaling, including single, trumpet-shaped and triple cotyledons, impaired vascular pattern, reduced vegetative growth, defective silique development and drastically reduced fertility. We demonstrate that AP2 σ is closely associated and physically interacts with the clathrin light chain (CLC) *in vivo* using fluorescence cross-correlation spectroscopy (FCCS), protein proximity analyses and co-immunoprecipitation assays. Using variable-angle total internal reflection fluorescence microscopy (VA-TIRFM), we show that AP2 σ-mCherry spots colocalize with CLC-EGFP at the plasma membrane, and that AP2 σ-mCherry fluorescence appears and disappears before CLC-EGFP fluorescence. The density and turnover rate of the CLC-EGFP spots are significantly reduced in the *ap2 σ* mutant. The internalization and recycling of the endocytic tracer FM4-64 and the auxin efflux carrier protein PIN1 are also significantly reduced in the *ap2 σ* mutant. Further, the polar localization of PIN1-GFP is significantly disrupted during embryogenesis in the *ap2 σ* mutant. Taken together, our results support an essential role of AP2 σ in the assembly of a functional AP2 complex in plants, which is required for clathrin-mediated endocytosis, polar auxin transport and plant growth regulation.

KEY WORDS: AP2 complex, AP-2, Clathrin-mediated endocytosis, FCCS, PIN auxin transporter, VA-TIRFM

INTRODUCTION

Endocytosis is the inward budding of the plasma membrane to form membrane vesicles, which are then transported to various subcellular compartments, and is the means by which cells take up extracellular materials, plasma membrane proteins and lipids (Conner and Schmid, 2003). In animal cells, endocytosis plays an essential role in signal transduction by specifically internalizing cell surface receptors to deactivate the response of cells to an extracellular stimulus (Sorkin and von Zastrow, 2009; McMahon and Boucrot, 2011). Clathrin-mediated endocytosis is the principal route by which cells internalize the transmembrane receptors (Doherty and McMahon, 2009; Taylor et al., 2011). Increasing evidence has demonstrated that clathrin-mediated endocytosis regulates cellular homeostasis, synaptic transmission and cell differentiation by controlling constitutive and stimulated internalization of many receptors (McMahon and Boucrot, 2011). Bacterial and viral toxins also enter cells through this pathway (Chen and Zhuang, 2008; Cureton et al., 2009; Abrami et al., 2010).

During clathrin-mediated endocytosis, clathrin-coated vesicle (CCV) formation and cargo selection require endocytic adaptor proteins. Two classes of adaptors have been identified based on different functions in clathrin-mediated endocytosis: the monomeric adaptor proteins (such as AP180, epsin and β-arrestin) and the heterotetrameric adaptor protein complexes, such as the AP2 (or AP-2) adaptor complex (Owen et al., 2004; Robinson, 2004). The AP2 complex is the main component among endocytic vesicle coat proteins, second in abundance only to clathrin itself (Schmid and McMahon, 2007; Kelly and Owen, 2011), and can link membrane cargo containing YXXØ-type sorting signals to the endocytic vesicle via binding of the μ2 subunit (Kelly et al., 2008; Traub, 2009). Recent experiments have shown that the α and σ2 subunits form a hemicomplex that interacts with the [DE]XXXL[LI] sorting signal and is also involved in the selective internalization of cargo proteins (Doray et al., 2007; Diril et al., 2009). Moreover, crystallography has identified the σ2 subunit as the major interaction site (Jackson et al., 2010).

The plant genome encodes proteins homologous to those that participate in clathrin-mediated endocytosis in mammalian cells. However, the molecular machinery of clathrin-mediated endocytosis in the plant cell is still uncharacterized (Samaj et al., 2005; Bassham et al., 2008). Recent studies indicate that clathrin-dependent endocytosis exists in plant cells and participates in many fundamental cellular processes (Pérez-Gómez and Moore, 2007; Kaiserli et al., 2009; Chen et al., 2011). Sequence analysis has suggested that *Arabidopsis* possesses four AP complexes (AP1, AP2, AP3 and AP4), which might be involved in different intracellular trafficking processes (Happel et al., 2004; Bar et al., 2009; Feraru et al., 2010; Zwiewka et al., 2011). Recently, a fifth adaptor protein (AP5) was identified. AP5 is localized on late endosomes and may be involved in endosomal dynamics (Hirst et al., 2011; Hirst et al., 2013). Although the AP2 complex is not essential for clathrin-mediated endocytosis in yeast (Yeung et al., 1999), it is involved in the internalization of membrane proteins in mammalian cells (Motley et al., 2003; Huang et al., 2004; Boucrot et al., 2010). The role of the homologous complex in plants has yet to be investigated.

[1]Key Laboratory of Plant Molecular Physiology, Institute of Botany, Chinese Academy of Sciences, Beijing 100093, China. [2]Graduate University of Chinese Academy of Sciences, Beijing 100049, China. [3]College of Life Science, Henan Normal University, Xinxiang 453007, China. [4]School of Life Sciences, Shandong University, Jinan 250100, China. [5]Departamento de Biología Celular, Genética y Fisiología, Universidad de Málaga, 29071 Malaga, Spain. [6]Department of Molecular, Cellular, and Developmental Biology, Yale University, New Haven, CT 06520-8104, USA.

*These authors contributed equally to this work
‡Author for correspondence (linjx@ibcas.ac.cn)

Accepted 2 July 2013

In this study, we identified and characterized the putative σ subunit of the AP2 complex, a novel adaptor of the clathrin-mediated endocytic machinery in *Arabidopsis*. We found that *Arabidopsis AP2 σ* was ubiquitously expressed, with a protein distribution at both the plasma membrane and in the cytoplasm. A loss-of-function *ap2 σ* mutant was impaired in endocytosis, showing defects in multiple aspects of plant development. Co-immunoprecipitation and fluorescence cross-correlation spectroscopy (FCCS) analyses showed that AP2 σ interacts with clathrin light chain (CLC) *in vivo*. To investigate the molecular dynamics at high spatiotemporal resolution on the plasma membrane, we made used of variable-angle total internal reflection fluorescence microscopy (VA-TIRFM) combined with a single-particle tracking (SPT) assay (Li et al., 2011; Wan et al., 2011) to reveal that AP2 σ displays similar dynamic behavior to CLC and accumulates at the endocytic clathrin-coated pits (CCPs). These findings provide new insight into the machinery and function of clathrin-mediated endocytosis in plant cells.

MATERIALS AND METHODS

Plant materials and growth conditions

Arabidopsis thaliana plants of ecotype Colombia-0 (Col-0) were used in all experiments. Seeds were surface sterilized in 75% ethanol for 10 minutes, washed five times with 95% ethanol, then plated on half-strength Murashige and Skoog (MS) medium (Murashige and Skoog, 1962) containing 1% (w/v) sucrose and 0.9% (w/v) agar (Duchefa, The Netherlands) and grown vertically at 22°C under a light regime of 16 hours light and 8 hours dark. An *ap2 σ* T-DNA insertion mutant was purchased from ABRC. The genotype of the *ap2 σ* insertion line was determined by PCR and confirmed by RT-PCR. Primers for T-DNA insertion mutant identification and RT-PCR are listed in supplementary material Table S3.

Construction of plasmids

The CLC-EGFP and AP2 σ-EGFP plant expression vectors were constructed as follows. The *CLC* and *AP2 σ* sequences, which included the promoter elements and coding regions, were PCR amplified from *Arabidopsis* genomic DNA with primers CLC_for/CLC_rev and AP2 σ_for/AP2 σ_rev and then subcloned as *Pst*I-*Spe*I and *Pst*I-*Kpn*I fragments into PM999-EGFP (kindly provided by Jian Xu, National University of Singapore) to produce PM999-CLC-EGFP and PM999-AP2 σ-EGFP, respectively. The CLC_rev and AP2 σ_rev primers contained linker sequences encoding Gly-Gly-Gly-Gly-Ala that appended the CLC and AP2 σ genomic fragment onto the N-terminus of EGFP. After digestion with *Pst*I and *Sma*I, the fragments of PM999-CLC-EGFP and PM999-AP2 σ-EGFP that included the genomic fragments of CLC/AP2 σ, EGFP and NOS were subcloned into the binary vector pCambia 1301 (CAMBIA, Canberra, Australia) to obtain pCambia 1301-CLC-EGFP and pCambia 1301-AP2 σ-EGFP.

To create the AP2 σ-mCherry expression vector, the coding sequence for mCherry was amplified using mCherry_for/mCherry_rev and then subcloned as a *Kpn*I/*Bam*HI fragment into pCambia 1301-AP2 σ-EGFP to replace EGFP, producing pCambia 1301-AP2 σ-mCherry.

Primers used for plasmid construction are listed in supplementary material Table S3.

Phenotype analysis

Cotyledon veins of 7-day-old seedlings were observed. The cotyledons were cleared in 100% ethanol overnight to remove chlorophyll and then mounted on slides containing 70% lactic acid. For analysis of developmental defects of embryos, developing seeds were cleared in an 8:3:1 (w:v:v) mixture of chloral hydrate:water:glycerol and observed on a Zeiss LSM 510 META microscope under differential interference contrast optics. For transmission electron microscopy (TEM), the samples were prepared according to a standard procedure (Luft, 1961) and examined under an FEI Tecnai Spirit microscope.

Fluorescence recovery after photobleaching (FRAP) analysis

FRAP experiments were performed on an FV1000MPE multiphoton laser-scanning microscope (Olympus). A rectangular region of interest was drawn around the area for bleaching by 488-nm laser lines operating at 100% laser power. The fluorescence recovery was monitored at 2-second intervals. The fluorescence recovery data obtained were corrected for bleaching during imaging as described (Konopka et al., 2008).

FM4-64 internalization assay

To evaluate the rate of endocytosis, the fluorescent styryl membrane probe FM4-64 (Invitrogen) was used. FM4-64 was kept as a 5 mM stock solution and diluted with half-strength liquid MS medium to produce a 5 μM working solution. Wild-type and *ap2 σ* seedlings were grown on half-strength MS plates for 3 days and then incubated in FM4-64 working solution for 5 minutes at room temperature. The seedlings were washed three times in half-strength liquid MS medium and transferred to glass slides. The internalization of FM4-64 was monitored at 5-minute or 30-minute intervals at room temperature using a Leica TCS SP5 II laser-scanning confocal microscope.

Co-immunoprecipitation and immunoblot analysis

To monitor the expression of the AP2 σ-EGFP fusion protein in transgenic plants, total proteins were extracted from *AP2 σ-EGFP* and *35S::EGFP* transgenic seedlings grown on half-strength MS plates. The seedlings were ground into a fine powder in liquid nitrogen, mixed in a 1:1 (v:v) ratio with SDS-PAGE sample buffer, heated at 95°C for 15 minutes and then centrifuged at 12,000 rpm (10,625 ***g***) for 5 minutes to remove cellular debris. The supernatants were subjected to 10% SDS-PAGE. Immunoblot analysis was performed with monoclonal anti-GFP antibody (Sigma-Aldrich). Horseradish peroxidase (HRP)-conjugated anti-mouse secondary antibody (Sangon Biotech, Shanghai, China) was used to detect the primary antibody.

For co-immunoprecipitation, 1 g of 10-day-old transgenic plants expressing CLC-EGFP, AP2 σ-mCherry and CLC-EGFP/AP2 σ-mCherry were harvested and ground in liquid nitrogen. The co-immunoprecipitation assay was performed as previously described (Serino and Deng, 2007).

Drug treatment and plasmolysis

TyrA23, TyrA51 and BFA (Sigma-Aldrich) were dissolved in DMSO to yield a 50 mM stock solution. For drug treatment, vertically grown seedlings were incubated in half-strength liquid MS medium containing 50 μM TyrA23 or 50 μM BFA at room temperature for the indicated time before VA-TIRFM or laser-scanning confocal microscopy analysis. Control cells were treated with equivalent amounts of DMSO.

Plasmolysis was carried out by incubating 4-day-old seedlings in 1 M NaCl for 5 minutes before observation.

FCCS analysis

FCCS measurements were carried out on the Leica TCS SP5 microscope. To avoid overestimation of cross-correlation, a low-power excited laser was used to prevent bleed-through between channels. The emitted signal was detected by avalanche photodiodes (APD) and transferred to a second computer where it was analyzed with ISS VISTA software. The fluorescence autocorrelation functions of the red $G_r(\tau)$ and green $G_g(\tau)$ channels, as well as the cross-correlation function $G_c(\tau)$, were calculated using the integrated function within ISS VISTA, where τ denotes the time delay. The acquired $G_r(\tau)$, $G_g(\tau)$ and $G_c(\tau)$ data were fitted to a 2D-Gaussian, two-particle type model. The relative cross-correlation ($[G_c(0)]/[G_g(0)]$ and $[G_c(0)]/[G_r(0)]$) was obtained by normalizing the amplitude of the cross-correlation function to the amplitude of the autocorrelation function of CLC-EGFP or AP2 σ-mCherry.

VA-TIRFM live imaging and data analysis

Seedlings were grown on half-strength MS agar plates and cultured vertically at 22°C for 3 days, then mounted on a glass slide with half-strength liquid MS medium and observed under a home-built VA-TIRF microscope, which was based on an Olympus IX-71 microscope equipped with a ×100 oil-immersion objective (numerical aperture of 1.45, Olympus) and makes use of subcritical incident angles of the laser to image the dynamics of fluorescently labeled proteins in plant epidermal cells. A diode laser (Changchun New Industries Optoelectronics Tech. Co., Changchun, China) was used for illumination through a total internal reflection

illuminator. EGFP- and mCherry-labeled proteins were excited with 473-nm and 561-nm laser lines and the emission fluorescence signals were passed through two band-pass filters (525/45 and 609/54 nm) before being detected by a back-illuminated EM-CCD camera (ANDOR iXon DV8897D-CS0-VP; Andor Technology, Belfast, UK). Images were acquired using a 200-msecond exposure time at 1-second intervals and were processed using ImageJ software (NIH). To analyze the dynamic properties, AP2 σ-EGFP and CLC-EGFP spots were tracked using spatial and temporal global particle assignment as described (Jaqaman et al., 2008).

Accession numbers

Sequence data used in this study are available from the *Arabidopsis* Information Resource (TAIR) database under accession numbers At2g40060 (CLC) and At1g47380 (AP2 σ).

RESULTS

The *ap2 σ* mutant exhibits defects in plant development

To characterize the function of AP2 σ in *Arabidopsis*, we first performed phylogenetic analysis using Molecular Evolutionary Genetics Analysis (MEGA) 4. Our analysis showed that the *Arabidopsis* genome contains a single gene for AP2 σ, which is closely related to animal AP2 σ (supplementary material Fig. S1A). In addition, AP2 σ is highly conserved across the fungal, animal and plant kingdoms (supplementary material Fig. S1B). Sequence alignment analysis further revealed that AP2 σ shares high similarity (61% identity) with human AP2 σ (AP2S1) (supplementary material Fig. S1C).

We obtained the AP2 σ heterozygous T-DNA insertion mutant (SALK_141555) from the *Arabidopsis* Biological Resource Center (ABRC) and screened for the homozygous line (Fig. 1A). We could not detect *AP2 σ* transcripts in the homozygous mutant by RT-PCR using primers flanking the T-DNA insertion site (Fig. 1B). Phenotypic analysis showed that multiple stages of plant growth and developmental processes were disturbed in the *ap2 σ* mutant. Most strikingly, the cotyledons exhibited defective organogenesis, and 19.6% of the seedlings had single, triple or fused cotyledons (Fig. 1C-G; supplementary material Table S1). Moreover, the abnormal cotyledon was also associated with an altered vascular pattern. In the wild type, the vascular tissues of the cotyledons formed closed networks (supplementary material Fig. S2A). By contrast, the cotyledons of the *ap2 σ* mutant exhibited an open vascular network, which was characterized by an increase in free-ending veins (supplementary material Fig. S2B-D). When grown in soil, the *ap2 σ* mutant seedlings exhibited dwarf phenotypes, with reduced leaf size and stem height (Fig. 1H,I). In addition, the dwarf seedlings also produced shorter siliques than wild-type plants (Fig. 1J,K): the average silique lengths were 12.49±1.60 mm for the wild type and 3.77±0.54 mm for the *ap2 σ* mutant (Fig. 1L).

To confirm that the developmental defects in the T-DNA mutant were caused by the loss of AP2 σ function, we transformed an AP2 σ-EGFP translational fusion construct into the *ap2 σ* mutant. Immunoblot analysis showed that AP2 σ was expressed as a fusion protein with EGFP (supplementary material Fig. S3A). Importantly, the transformation of the *ap2* σ mutant with AP2 σ-EGFP fully rescued the developmental defects (supplementary material Fig. S3B-D). These results indicate that AP2 σ-EGFP is functional and that AP2 σ is required for normal plant growth and development.

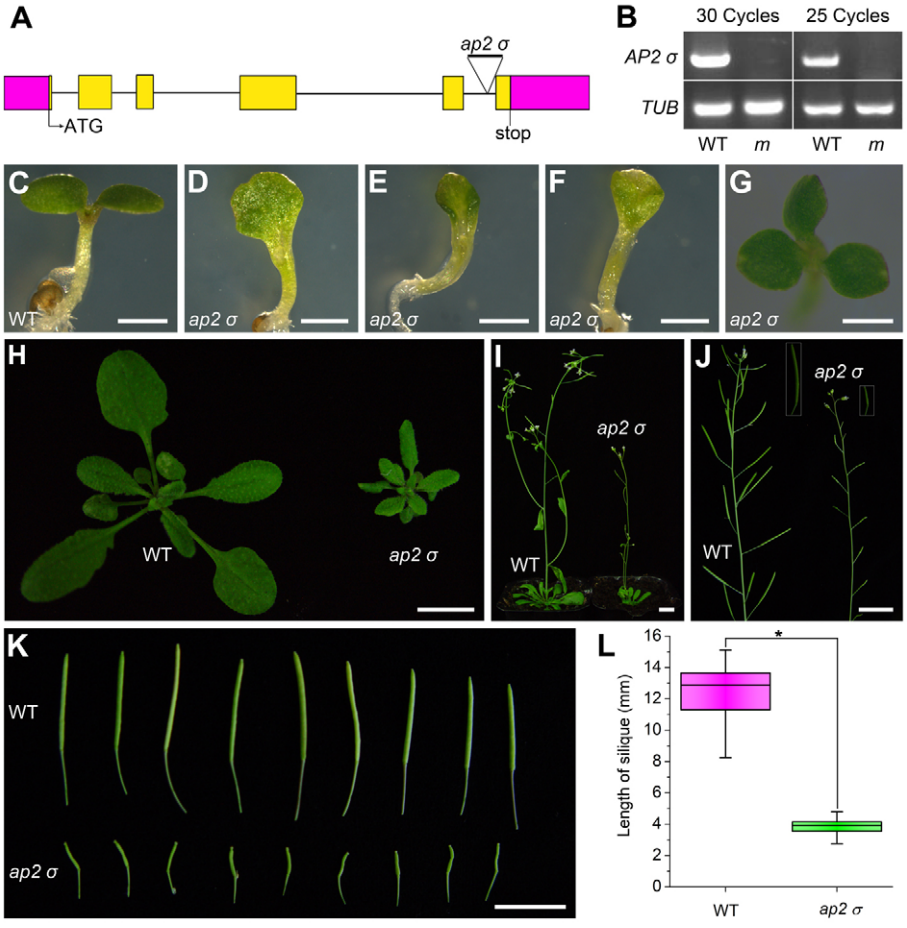

Fig. 1. AP2 σ is required for multiple stages of growth and development in *Arabidopsis*. (**A**) *AP2 σ* gene structure. Magenta boxes, orange boxes and bars represent UTRs, exons and introns, respectively. The triangle indicates the T-DNA insertion site. (**B**) Semi-quantitative RT-PCR analysis of *AP2 σ* expression in the wild type (WT) and the *ap2 σ* mutant (*m*). The PCR product of *AP2 σ* is 516 bp. RT-PCR cycle numbers are indicated. *β-TUBULIN* (*TUB*) was used as internal control. (**C-G**) Four-day-old seedlings of the wild type (C) and the *ap2 σ* mutant with single (D), trumpet-shaped (E,F) and triple (G) cotyledons. (**H**,**I**) Three-week-old (H) and 5-week-old (I) wild-type and *ap2 σ* mutant plants. (**J**) Inflorescences of the wild type and the *ap2 σ* mutant. (**K**) Comparison of silique lengths in the wild type and the *ap2 σ* mutant. (**L**) Box plot of silique length of the wild type (*n*=43) and the *ap2 σ* mutant (*n*=45). Boxes represent the 25-75% quartiles; the bar in the box represents the median (50% quartile); whiskers extend out to 1.5 times the interquartile range. **P*<0.01, Student's *t*-test. Scale bars: 1 mm in C-G; 10 mm in H-K.

The *ap2 σ* mutant shows disrupted localization and reduced endocytosis of the PIN1 auxin transporter

Given the prominent defect in cotyledon formation, we investigated embryo development in the *ap2 σ* mutant. In contrast to the wild type (Fig. 2A-C), we observed abnormal embryo shapes at the globular stage in the *ap2 σ* mutant (Fig. 2D). In the heart and torpedo stages, single cotyledon primordium was visible in *ap2 σ* mutant embryos (Fig. 2E,F). Moreover, the distribution of *DR5::GFP* (a synthetic auxin reporter) was altered in the tip of incipient cotyledons of ap2 σ mutant embryos (Fig. 2G-L), indicating that the distribution of auxin is disrupted.

As the establishment of correct auxin maxima and formation of a normal bilateral axis depend on the polar localization of the auxin efflux transporter PIN1 in the embryo, we next compared the localization of a functional PIN1-GFP fusion protein in the wild type and *ap2 σ* mutant. PIN1-GFP was expressed throughout the wild-type embryo, with higher expression in the apical and central region of the globular embryo. At the heart stage, PIN1-GFP was restricted to the vascular precursor cells, with higher levels at the basal boundary towards the site of the future root tip. The opposite polarity was observed in the protodermal cell layer of cotyledon primordia (Fig. 3A-D). In the *ap2 σ* mutant, PIN1-GFP was mainly localized in the region of the cotyledon and vasculature initiation sites at the globular and heart stages, but the subcellular localization of PIN1-GFP was significantly disrupted. The polar localization of PIN1-GFP was lost, accompanied by large aggregations in the membrane-associated regions (Fig. 3E-H).

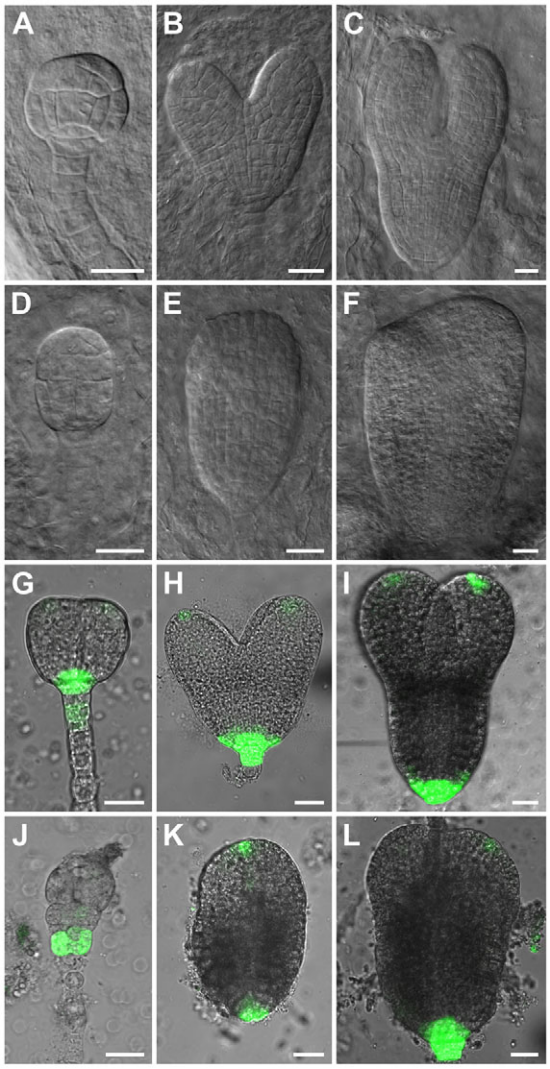

Fig. 2. Embryo defects and disrupted auxin distribution in the *ap2 σ* mutant. (**A-F**) Wild-type (A-C) and *ap2 σ* mutant (D-F) embryos at (A,D) early globular stage, (B,E) heart stage and (C,F) torpedo stage. (**G-L**) *DR5::GFP* distribution in wild-type (G-I) and *ap2 σ* mutant (J-L) embryos at the globular stage (G,J), heart stage (H,K) and torpedo stage (I,L). Scale bars: 20 μm.

Considering that PIN1 undergoes constitutive clathrin-dependent endocytosis and recycling between plasma membrane and endosomes (Dhonukshe et al., 2007; Dhonukshe et al., 2008), we investigated the effects of the *ap2 σ* mutation on its internalization. To visualize PIN1-GFP endocytosis, we inhibited endocytic recycling using the fungal toxin brefeldin A (BFA), which causes the heterogeneous aggregation of internalized PIN1 in intracellular compartments (known as 'BFA bodies') (Pan et al., 2009; Naramoto et al., 2010). As expected, the aggregation of PIN1-GFP in BFA bodies was clearly observed in the wild type when treated with BFA (Fig. 3I). Although BFA treatment also caused the formation of PIN1-GFP aggregates, the formation of BFA bodies was remarkably reduced in the *ap2 σ* mutant (Fig. 3J). Further statistical analysis revealed that the fluorescence intensity and size of the PIN1-GFP-labeled BFA bodies decreased by 25% and 45%, respectively, in the *ap2 σ* mutant as compared with the wild type (Fig. 3K,L). Colocalization and FCCS analysis further revealed that PIN1-GFP was associated with AP2 σ-mCherry (supplementary material Fig. S4A,B). Immunoblot analysis demonstrated that there were no differences in PIN1-GFP protein levels between the wild type and the *ap2 σ* mutant, ruling this out as having any effect on PIN1 internalization and localization (supplementary material Fig. S5A). These results indicate that AP2 σ is required for the proper internalization of PIN1.

Plasma membrane and cytoplasmic localization of AP2 σ

Microarray data (publicly available via Genevestigator, https://www.genevestigator.com) show that *AP2 σ* is ubiquitously expressed in all tissues and throughout all developmental stages and that its expression level is barely affected by the factors analyzed in the microarray data (Zimmermann et al., 2004). Live cell imaging revealed the AP2 σ-EGFP fluorescence signal as a thin layer at the cell periphery in all cell types analyzed, although some fluorescence was also observed in the cortical region of the cells (supplementary material Fig. S6A-D). To further examine whether the AP2 σ-EGFP fluorescent signals are localized to the plasma membrane, periplasmic space or cell wall, we performed a plasmolysis experiment with 1 M NaCl treatment before confocal imaging. A substantial fraction of the AP2 σ-EGFP fluorescent signal remained associated with the shrunken plasma membrane, with little residual signal in the cell walls of the plasmolyzed root epidermal cells (supplementary material Fig. S7). These results indicate that AP2 σ-EGFP is localized both at the plasma membrane and in the cytoplasm.

To study how AP2 σ-EGFP is recruited to the plasma membrane, we examined the dynamics of AP2 σ-EGFP in the subapical lateral plasma membrane of growing root hairs using FRAP. The initial bleaching region was divided into three parts designated as the top, middle and bottom sectors (Fig. 4A). Our FRAP experiment showed that the three regions recovered at equal rates (Fig. 4A,B), with a similar average half-life and percentage recovery (supplementary

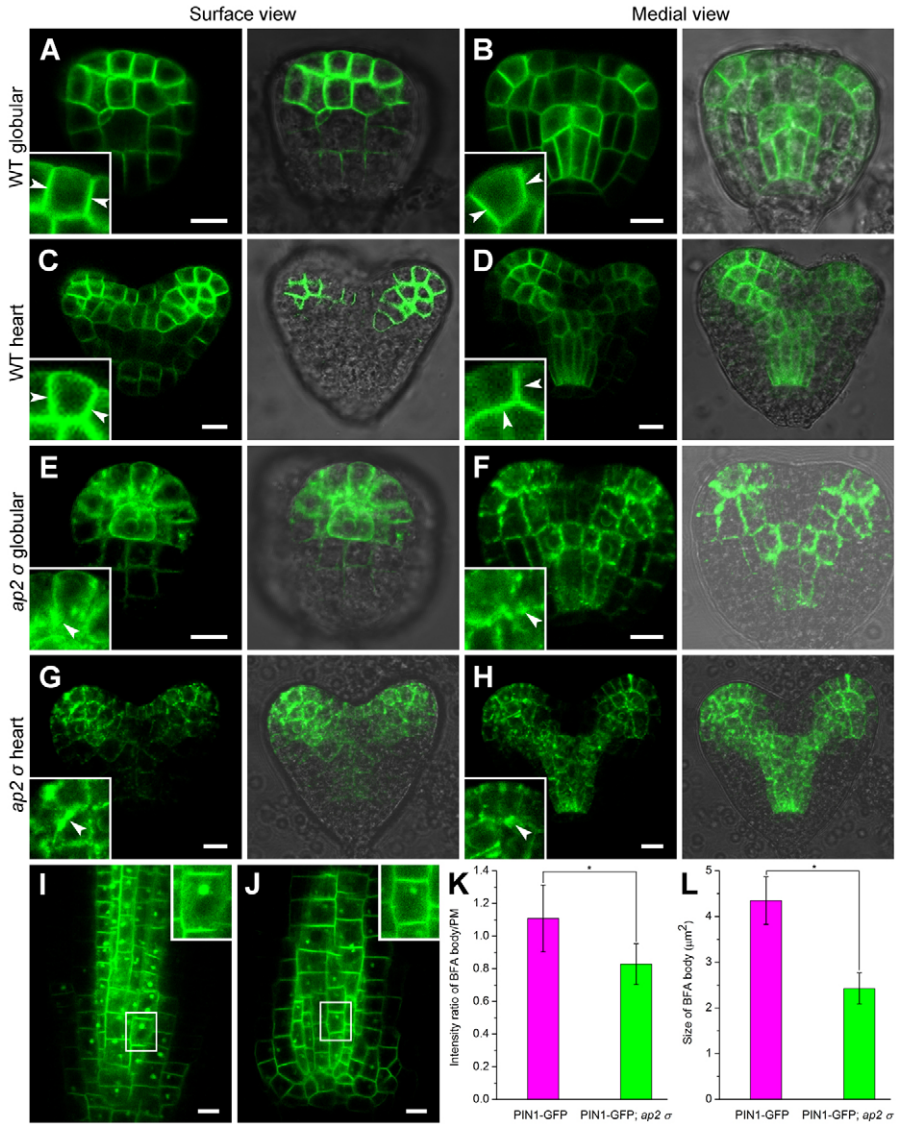

Fig. 3. PIN1 subcellular localization and internalization are disrupted in the *ap2 σ* mutant. (**A-H**) PIN1-GFP localization in globular stage (A,B,E,F) and heart stage (C,D,G,H) wild-type (A-D) and *ap2 σ* mutant (E-H) embryos. Arrowheads in high-magnification insets indicate the normal and disrupted localization of PIN1-GFP in the wild type and the ap2 σ mutant, respectively. (**I**,**J**) PIN1-GFP-labeled BFA bodies in the wild type (I) and *ap2 σ* mutant (J). Insets show higher magnification views of BFA bodies in the wild type and the ap2 σ mutant. (**K**) Signal intensities of PIN1-GFP-labeled BFA bodies in the wild type and *ap2 σ* mutant. (**L**) Sizes of PIN1-GFP-labeled BFA bodies in the wild type and *ap2 σ* mutant. (K,L) n=10 roots with at least 120 BFA bodies. *P<0.01, Student's t-test. Mean ± s.d. Scale bars: 10 μm.

material Table S2), suggesting that AP2 σ-EGFP is primarily recruited from the cytoplasm to the plasma membrane.

The *ap2 σ* mutant is defective in endocytosis

To test whether the AP2 complex plays a role in endocytosis in *Arabidopsis*, we examined the uptake of the commonly used endocytic tracer FM4-64 in the wild type and *ap2 σ* mutant (Fig. 5A,B). In the wild type, FM4-64-labeled fluorescent puncta could be detected in the cytoplasm 5 minutes after labeling, whereas in the *ap2 σ* mutant little FM4-64 uptake could be detected even 25 minutes after labeling (Fig. 5C,D).

To determine the endocytic rate, we monitored the internalization of FM4-64 on a long time scale. Thirty minutes after labeling, the internalization of the dye was obvious in wild-type roots; by contrast, no dye accumulation was apparent in the *ap2 σ* mutant. One hour after labeling, a large number of FM4-64-labeled vesicles were detected in the cytoplasm of wild-type cells, whereas in the *ap2 σ* mutant only limited cytoplasmic fluorescence was detected even 90 minutes after labeling (supplementary material Fig. S8). The effect of AP2 σ on endocytosis was further confirmed by rescue of the FM4-64 internalization rate in the complementation lines (supplementary material Fig. S9A,B).

AP2 σ associates with CLC *in vivo* at the plasma membrane

To gain further insight into the molecular nature of the endocytic defect of the *ap2 σ* mutant, we investigated the colocalization of AP2 σ and CLC. We generated transgenic plants co-expressing CLC-EGFP and AP2 σ-mCherry driven by their native promoters. Confocal imaging analysis showed a high level of CLC-EGFP and AP2 σ-mCherry overlap at the plasma membrane (Fig. 6A-C), as confirmed by quantitative analysis [the protein proximity index (PPI)] (Zinchuk et al., 2011). Fig. 6D is a 3D plot of the cross-correlation of CLC-EGFP and AP2 σ-mCherry as a function of pixel shift. The peak at the center of the 3D surface plot decreased significantly upon shifting the image a few pixels (Fig. 6D), indicating specific colocalization of CLC and AP2 σ. The mean PPI values were 0.69±0.15 for the proximity of CLC to AP2 σ and 0.62±0.13 for the proximity of AP2 σ to CLC (Fig. 6E).

The possible interaction between CLC and AP2 σ was then investigated using co-immunoprecipitation and FCCS. AP2 σ-mCherry was co-immunoprecipitated with CLC-EGFP in transgenic plants co-expressing the two proteins, indicating that AP2 σ interacts with CLC *in vivo* (supplementary material Fig. S10). The interaction between AP2 σ and CLC was further analyzed using

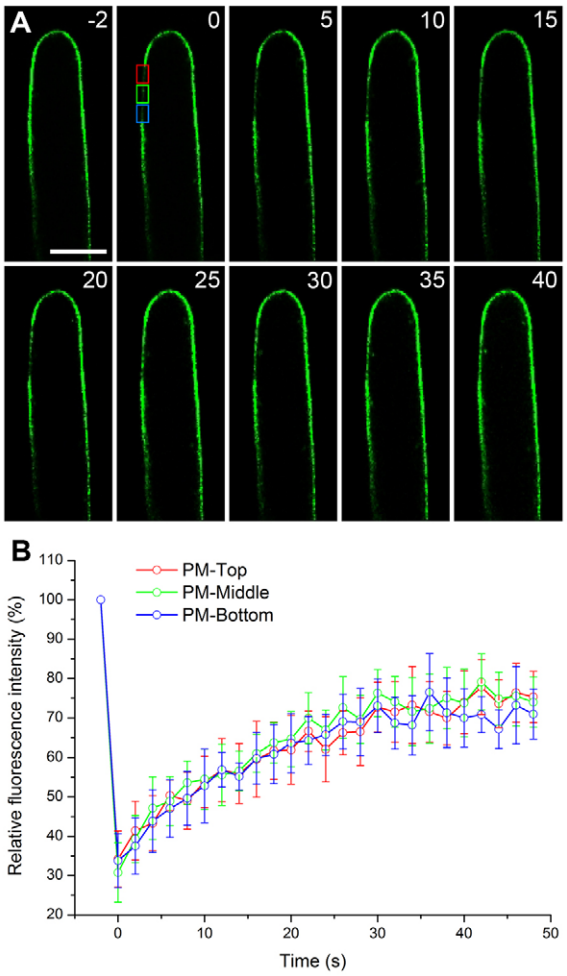

Fig. 4. Dynamic analysis of AP2 σ-EGFP at the plasma membrane of growing root hairs using FRAP. (**A**) Timecourse of FRAP of AP2 σ-EGFP. The initial bleaching region was subdivided into three sectors, as indicated by the red, green and blue squares. Time is given in seconds. (**B**) Fluorescence recovery curve for a dataset of ten independent FRAP experiments on AP2 σ-EGFP. Error bars indicate s.d. Scale bar: 10 μm.

FCCS. For each dataset, the amplitude of cross-correlation was compared with the green (CLC-EGFP) or red (AP2 σ-mCherry) autocorrelation amplitude, which represented the percentage of molecules associated with each other. A strong association was indeed observed between CLC-EGFP and AP2 σ-mCherry in living cells, and the cross-correlation values were 0.61±0.13 for CLC to AP2 σ and 0.63±0.14 for AP2 σ to CLC (Fig. 6F,G). Moreover, we found that both tyrphostin A23 (TyrA23), an inhibitor of clathrin-dependent endocytosis, and its inactive analog tyrphostin A51 (TyrA51) had no significant effect on the association of the two proteins (supplementary material Fig. S11A-C).

AP2 σ-EGFP displays similar dynamic properties to CLC-EGFP at the plasma membrane

We then applied VA-TIRFM to analyze the dynamics of AP2 σ-EGFP at the plasma membrane. When transgenic plants expressing AP2 σ-EGFP were viewed under VA-TIRFM, the fluorophores appeared as small diffraction-limited fluorescent spots (Fig. 7A) and displayed similar dynamic behavior to CLC-EGFP, including the appearance into, and disappearance from, the focal plane (Fig. 7B-F). Interestingly, AP2 σ-EGFP exhibited some unique characteristics. Most of the AP2 σ-EGFP signals were diffraction-limited fluorescence spots, and no large puncta were observed in the AP2 σ-EGFP transgenic plants, whereas the cortical trans-Golgi network could be clearly detected in CLC-EGFP transgenic plants (Fig. 7A,C; supplementary material Movies 1, 2).

We further analyzed the dynamic behavior of AP2 σ-EGFP and CLC-EGFP by measuring their diffusion coefficients and mean velocities. The diffusion coefficients were calculated by performing a linear fit of the mean-squared displacement (MSD) versus time. Interestingly, the diffusion coefficients of AP2 σ-EGFP and CLC-EGFP were similar, both ranging from 10^{-3} μm^2/second to 1 μm^2/second. The $\hat{G}$ values (characteristic of diffusion coefficients) were 2.67×10^{-2} μm^2/second for AP2 σ-EGFP and 2.43×10^{-2} μm^2/second for CLC-EGFP (Fig. 7G,H). The two proteins also moved with similar velocities: $6.17\pm0.13\times10^{-1}$ μm/second for AP2 σ-EGFP and $5.94\pm0.065\times10^{-1}$ μm/second for CLC-EGFP (Fig. 7I,J).

To verify the relationship between AP2 σ and clathrin, we investigated the effects of TyrA23 on the dynamics of AP2 σ. When AP2 σ-EGFP transgenic *Arabidopsis* seedlings were treated with TyrA23, the number of AP2 σ-EGFP spots at the plasma membrane was significantly reduced. When the seedlings were treated with TyrA51, this effect was not observed (supplementary material Fig. S12A,B), indicating that AP2 σ-EGFP-labeled fluorescent spots were specifically sensitive to TyrA23, which is similar to its effect on the dynamin-related protein DRP1A during clathrin-mediated endocytosis in *Arabidopsis* (Fujimoto et al., 2010).

AP2 σ accumulates at endocytic CCP sites

Given that AP2 σ had a high cross-correlation with CLC and displayed very similar dynamics to CLC-EGFP at the plasma membrane, we next examined their dynamics at the plasma membrane by imaging plants co-expressing AP2 σ-mCherry and CLC-EGFP using dual-color VA-TIRFM. In root epidermal cells, the CLC-EGFP and AP2 σ-mCherry fusion proteins appeared as well-dispersed diffraction-limited fluorescent spots at the plasma membrane and the AP2 σ-mCherry fluorescent spots overlapped with those of CLC-EGFP. In addition, some fluorescent spots containing only GFP or mCherry signal were observed (Fig. 8A-C). Fig. 8D shows time-lapse imaging analysis of a single fluorescent spot exhibiting both green and red fluorescence. At t=5 seconds, the AP2 σ-mCherry fluorescence appears and increases rapidly, and then the CLC-EGFP fluorescence appears at the same site and colocalizes with the red signal (t=11.25 seconds). At t=35 seconds, the AP2 σ-mCherry fluorescence has disappeared and only the CLC-EGFP spot is still visible, until it disappears 2 seconds later. From the kymograph and a comparison of the fluorescence intensity profiles representing the CCP labeled by CLC-EGFP and AP2 σ-mCherry (Fig. 8E,F), it is obvious that the AP2 σ-mCherry fluorescence appeared and disappeared ahead of the CLC-EGFP fluorescence.

The localization and dynamics of CLC-EGFP are altered in the *ap2 σ* mutant

To provide further insight into the requirement of AP2 σ in clathrin-mediated endocytosis, we examined the localization and dynamics of CLC-EGFP in the *ap2 σ* mutant. Immunoblot analysis showed that the CLC-EGFP protein level in the wild type and *ap2 σ* mutant were similar (supplementary material Fig. S5B). Confocal analysis showed that CLC-EGFP was localized to the plasma membrane, intracellular structures (presumably the trans-Golgi network) and cytoplasm. However, the plasma membrane-associated CLC-EGFP

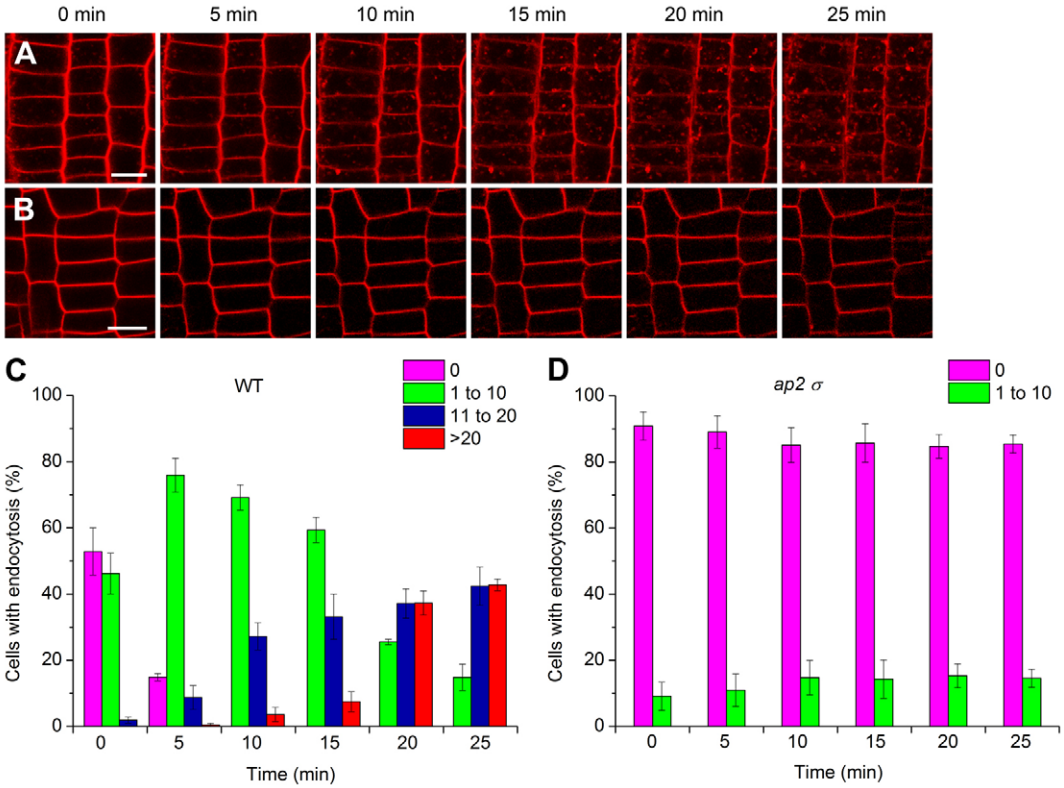

Fig. 5. Endocytosis of FM4-64 is reduced in the *ap2 σ* mutant. (**A**,**B**) Timecourse of FM4-64 internalization in the wild type (A) and *ap2 σ* mutant (B). (**C**,**D**) Quantification of endocytic vesicles in the (C) wild type (n=10 roots) and (D) *ap2 σ* mutant (n=12 roots). Cells are classified into four groups: cells with no vesicles in the cytoplasm; cells with 1-10 vesicles; cells with 11-20 vesicles; and cells with more than 20 vesicles. Mean ± s.d. Scale bars: 10 μm.

signal was significantly lower in the *ap2 σ* mutant than in wild-type seedlings (supplementary material Fig. S13A-C). Under VA-TIRFM, CLC-EGFP in the wild type was distributed in small spots at the plasma membrane and underwent constant internalization (Fig. 9A). In the *ap2 σ* mutant CLC-EGFP spots still formed, but the CCP density was significantly lower than in the wild type (0.65±0.13 μm^2 in the wild type versus 0.38±0.05 μm^2 in the *ap2 σ* mutant) (Fig. 9B,E; supplementary material Movie 3).

Because differences in CCP lifetime can affect their density, we further measured the turnover rate of CCPs. As shown in the kymograph, CLC-EGFP in the wild type was efficiently recruited to the plasma membrane, whereas the turnover rate was greatly reduced in the *ap2 σ* mutant (Fig. 9C,D). The appearance and disappearance rate of CLC-EGFP in the *ap2 σ* mutant decreased significantly to 70% of that in the wild type (Fig. 9F). TEM showed that 0.30±0.03% of the cell surface was occupied by CCVs in the wild type, whereas CCVs were less abundant in the *ap2 σ* mutant, occupying only 0.14±0.01% of the cell surface (supplementary material Fig. S14A-C).

DISCUSSION

Clathrin-mediated endocytosis is a highly dynamic process during which cell surface proteins and plasma membrane components are internalized into the cytoplasm. This process can be tracked in living cells using FM4-64, a membrane-selective fluorescent dye that can stain membrane in an activity-dependent manner (Leborgne-Castel et al., 2008; Men et al., 2008). Our results showed that depletion of AP2 σ function significantly inhibited the uptake of the dye, indicating that AP2 σ is required for general endocytic events in *Arabidopsis*. We also found that AP2 σ was ubiquitously expressed and mainly localized at the plasma membrane. Our FRAP analysis further showed that AP2 σ was directly recruited from the cytoplasm to the plasma membrane. Given the subcellular localization of AP2 σ-EGFP and the prominent interference of loss of function of AP2 σ in FM4-64 internalization in plant cells, we can safely conclude that AP2 σ represents one of the major adaptor proteins in *Arabidopsis*.

During clathrin-mediated endocytosis, more than 60 functionally distinct adaptor and accessory proteins are required, with functions ranging from clathrin recruitment and cargo sorting to membrane bending and vesicle scission (Maldonado-Báez and Wendland, 2006; Mettlen et al., 2009). Among these proteins, the AP2 complex was the first CCV adaptor to be characterized (Robinson, 1987; Collins et al., 2002). *Arabidopsis* AP180 has been identified as a clathrin assembly protein that binds to plant αC-adaptin (Barth and Holstein, 2004). To determine whether AP2 participates in the formation of CCVs in plants, we first analyzed the colocalization of fluorescently labeled AP2 with clathrin. Fluorescence microscopy images, although informative, cannot be used to precisely quantify protein colocalization owing to the possibility of false values resulting from the image background. In the present study, we applied a newly developed PPI to evaluate colocalization quantitatively in living cells (Li et al., 2010; Zinchuk et al., 2011). The PPI analysis revealed that AP2 σ has a high degree of colocalization with clathrin in living plant cells. Using the co-immunoprecipitation assay, we further demonstrated a direct physical interaction between AP2 σ and clathrin. This was supported by FCCS analysis, which yielded detailed quantitative information about the transient and dynamic interaction between AP2 σ-mCherry and CLC-EGFP (Bacia et al., 2006; Erdel et al., 2010; Fitzpatrick and Lillemeier, 2011). In cells expressing AP2 σ-

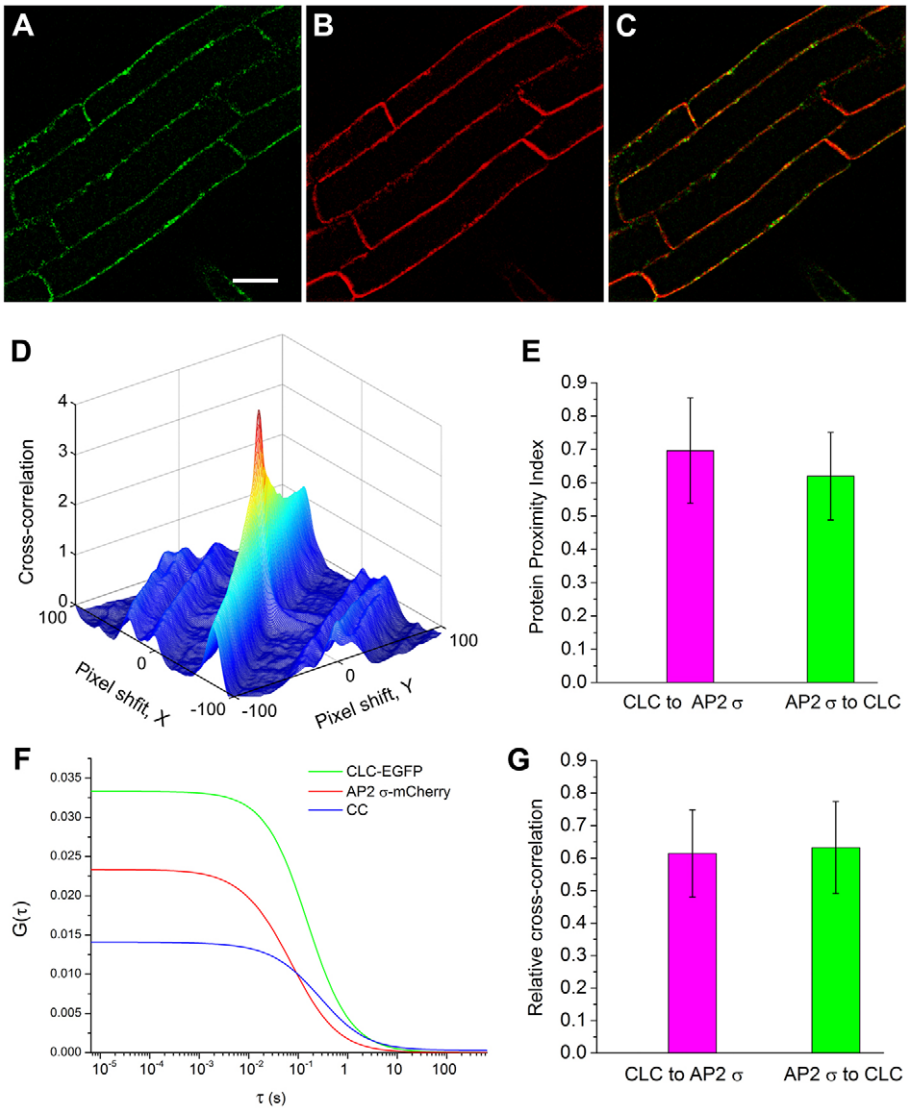

Fig. 6. Colocalization and interaction analysis of AP2 σ with CLC in living plant cells. (**A-C**) Confocal images of root epidermal cells expressing AP2 σ-mCherry (A) and CLC-EGFP (B) and merge (C). (**D**) Three-dimensional plot of CLC-EGFP and AP2 σ-mCherry cross-correlation versus pixel shift. (**E**) Mean protein proximity index values (*n*=10 images from 10 roots). (**F**) FCCS analysis of the cross-correlation between CLC-EGFP and AP2 σ-mCherry in living cells. (**G**) Cross-correlation values between CLC-EGFP and AP2 σ-mCherry (*n*=40 measurements from 12 roots). Mean ± s.d. Scale bar: 10 µm.

mCherry and CLC-EGFP, we observed a significant cross-correlation between AP2 σ and CLC in accordance with the colocalization data calculated using PPI. These comprehensive analyses provided strong evidence that AP2 σ and CLC exhibit a high-affinity interaction in living cells, indicating that AP2 σ serves as a key binding partner for clathrin.

Clathrin-mediated endocytosis is complex and dissecting how the multiple components in this process are spatially and temporally organized poses a challenge. VA-TIRFM is a type of microscopy that takes advantage of the unique property of the evanescent wave produced at the interface between the specimen and a glass coverslip and confines the excitation of the fluorophores to a depth of 100-400 nm in the specimen (Mattheyses et al., 2010; Wan et al., 2011). This provides a powerful approach to clarify spatially the details of complex kinetics at the single-molecule level in living plant cells (Ehrhardt and Frommer, 2012). From VA-TIRFM observations, we found that AP2 σ-EGFP formed discrete foci at the plasma membrane. SPT analysis showed that these foci displayed similar dynamics to those formed by CLC. Moreover, the localization of AP2 σ-EGFP at the plasma membrane was strongly disturbed by treatment with TyrA23. We could not rule out the possibility that TyrA23 acts as an inhibitor of tyrosine kinase to influence other cellular processes or that it inhibits the interaction between the tyrosine-based motif and other adaptor complexes, leading to the disruption of other membrane trafficking events (Banbury et al., 2003). Therefore, we examined the effect of TyrA51, an analog of TyrA23 with no influence on clathrin-mediated endocytosis, and found that it had no significant influence on the dynamic behavior of AP2 σ-EGFP. These observations further support the notion that AP2 σ and CLC are parts of the same endocytic machinery.

Clathrin-mediated endocytosis can be divided into five distinct stages in animal cells: initiation, assembly, maturation, vesicle scission and uncoating (McMahon and Boucrot, 2011). In the current investigation, we found that most of the AP2 σ-mCherry fluorescent foci visualized in the VA-TIRFM images also contained CLC-EGFP signal, confirming that AP2 σ colocalizes with CLC at the plasma membrane. In *ap2 σ* mutant cells, both the number and turnover rate of CLC-EGFP spots were significantly attenuated, indicating that AP2 σ promotes the formation of CLC-EGFP spots at the plasma membrane. Time-lapse imaging and kymograph analysis further revealed that the AP2 σ-mCherry fluorescence spots appeared and disappeared before the CLC-EGFP spots. Assuming that the above five stages of clathrin-mediated endocytosis exist in plant cells, we tentatively conclude that AP2 is involved in the CCV initiation, assembly and maturation stages, but is not necessary for

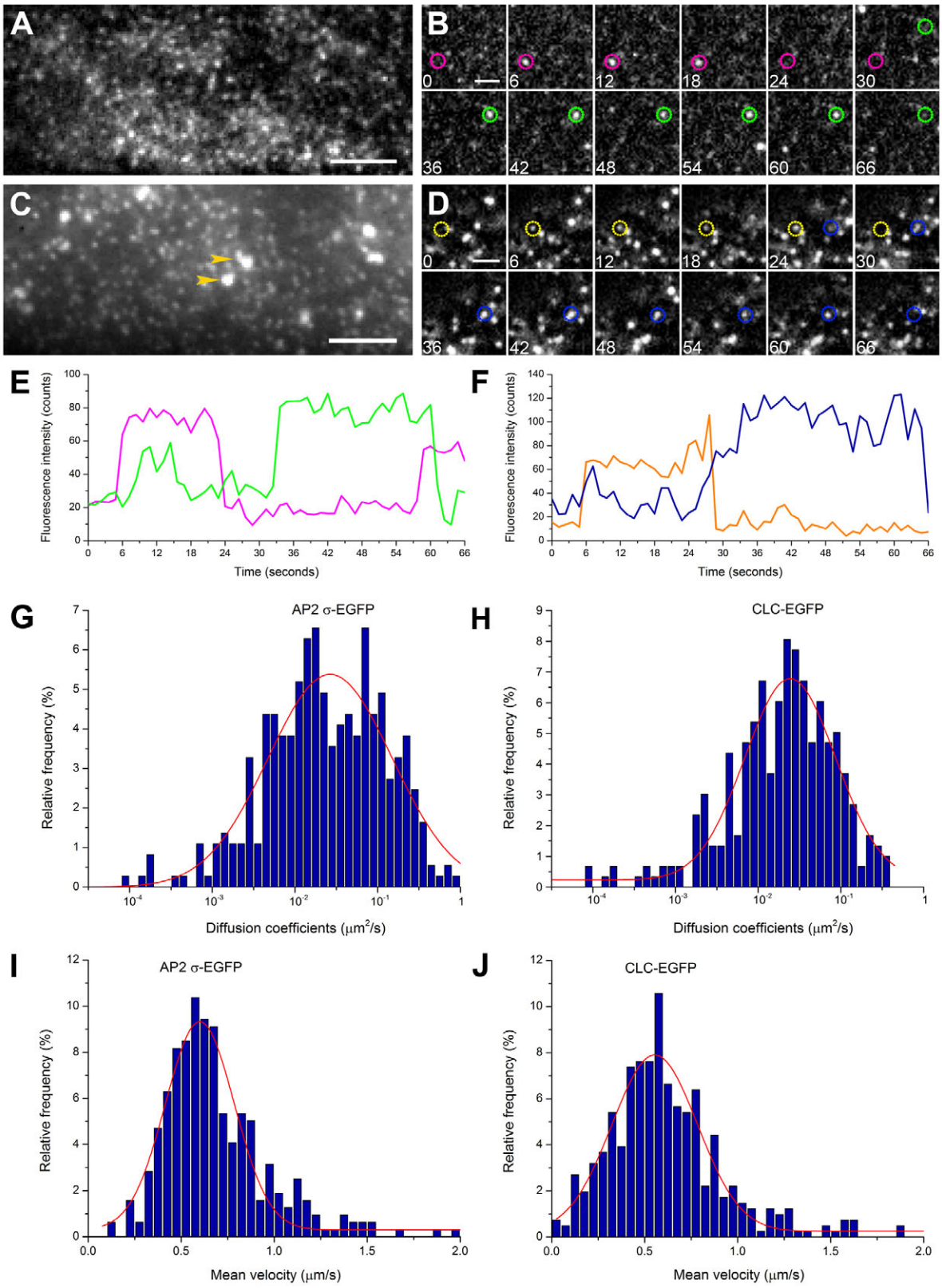

Fig. 7. Dynamic analysis of AP2 σ-EGFP and CLC-EGFP at the plasma membrane. (**A**) Live imaging of root epidermal cells expressing AP2 σ-EGFP using VA-TIRFM. (**B**) Images from a time series acquired at 1-second intervals showing that AP2 σ-EGFP is dynamic at the plasma membrane. Seconds elapsed from the beginning of image acquisition are indicated. (**C**) Live imaging of root epidermal cells expressing CLC-EGFP using VA-TIRFM. (**D**) Images from a time series acquired at 1-second intervals showing that CLC-EGFP is dynamic at the plasma membrane. Arrowheads indicate cortical Golgi. (**E**,**F**) Fluorescence intensity profiles of the two foci indicated in B and D, respectively. (**G**,**H**) Distribution of diffusion coefficients for AP2σ-EGFP (*n*=366 spots) and CLC-EGFP (*n*=261 spots) on the plasma membrane of epidermal cells. (**I**,**J**) Distribution of the mean velocity of AP2σ-EGFP (*n*=318 spots) and CLC-EGFP (*n*=407 spots) on the plasma membrane of epidermal cells. In G-J, the red lines indicate Gaussian fitting curves of the histogram. Scale bars: 5 μm in A,C; 2 μm in B,D.

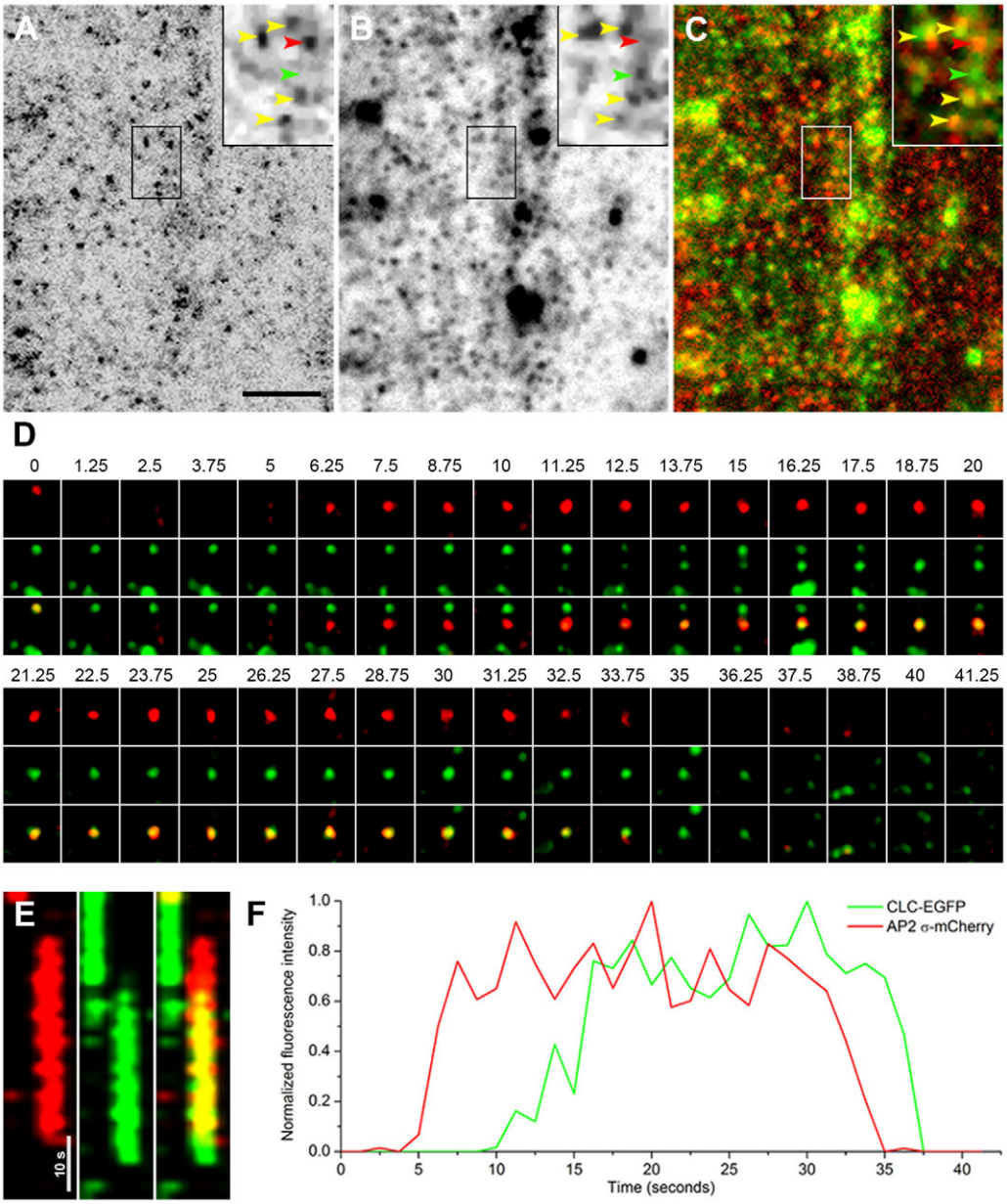

Fig. 8. Dual-color VA-TIRFM analysis of AP2 σ-mCherry and CLC-EGFP colocalization at the plasma membrane. (**A-C**) VA-TIRFM image of root epidermal cells expressing AP2 σ-mCherry (A) and CLC-EGFP (B) and merge (C). Four spots containing both GFP and mCherry fluorescence are indicated with yellow arrowheads in the high-magnification insets. The spots containing only GFP or mCherry are indicated with a green or red arrowhead, respectively. Scale bar: 5 µm. (**D**) Representative images of a spot containing AP2 σ-mCherry (top), CLC-EGFP (middle) and merge (bottom) over a timecourse (time shown in seconds). (**E**) Kymograph representation of the timecourse of green and red fluorescence. Left, middle and right represent AP2 σ-mCherry, CLC-EGFP and merge, respectively. (**F**) Time-normalized intensity profiles of AP2 σ-mCherry and CLC-EGFP of D.

the detachment of endocytic vesicles from the plasma membrane in *Arabidopsis*.

Some previous studies have focused on the role of AP2 in the regulation of embryonic development (Mitsunari et al., 2005; Yu et al., 2007). However, unlike its counterparts in animals, AP2 was considered a non-central player in clathrin-mediated endocytosis in yeast (Boettner et al., 2012). The experiments described here show that the loss-of-function *ap2 σ* mutant was impaired in many developmental processes, including embryo patterning, cotyledon organogenesis, vegetative growth and silique length. Among *ap2 σ* mutant seedlings 19.6% had single, triple or fused cotyledons with associated defective vascular patterns, resembling the phenotypes of auxin-related mutants (Mattsson et al., 2003; Furutani et al., 2004; Péret et al., 2012). More importantly, we found that the internalization of the auxin efflux carrier PIN1 was strongly inhibited and the polar localization of PIN1 on the plasma membrane was disrupted in the absence of AP2 σ. These observations suggest that AP2 might serve as a core adaptor linking clathrin and PIN1, through which PIN1 is internalized via the clathrin-dependent endocytic pathway, and that AP2 σ regulates cotyledon organogenesis by maintaining the proper localization of the auxin transporter.

The molecular and cellular studies presented here demonstrate that the AP2 complex is crucial for endocytosis and plant growth.

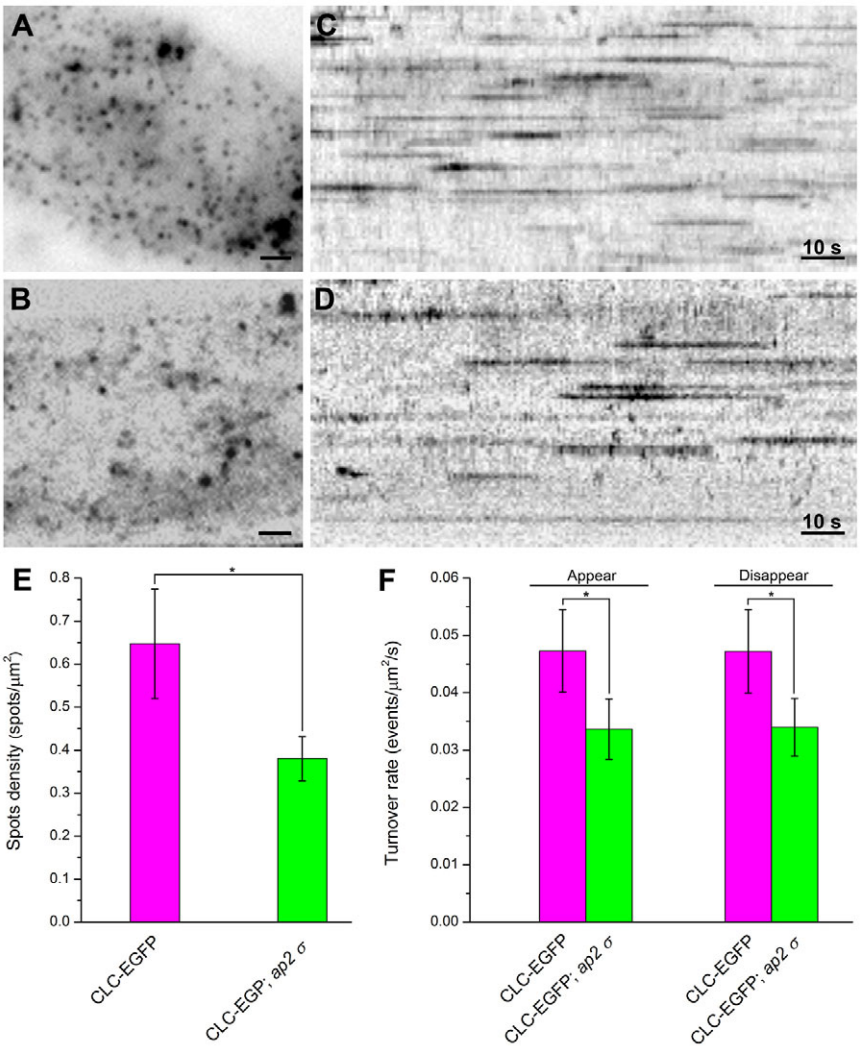

Fig. 9. The density and turnover rate of CLC-EGFP foci are diminished in the *ap2 σ* mutant. (**A**,**B**) VA-TIRFM image of root epidermal cells expressing CLC-EGFP in the wild type (A) and *ap2 σ* mutant (B). Scale bars: 2 μm. (**C**,**D**) Kymographs from representative time series images recorded at 1-second intervals in wild-type (C) and *ap2 σ* mutant (D) plants. (**E**) The densities of CLC-EGFP spots on the plasma membrane in the wild type and *ap2 σ* mutant. (**F**) Rates of appearance and disappearance of CLC-EGFP spots in the wild type and *ap2 σ* mutant. (E,F) n=12 roots. *P<0.01, Student's t-test. Mean ± s.d.

These findings might help address the potential role of clathrin-dependent endocytosis in the regulation of plasma membrane dynamics and signal transduction in plant cells.

Acknowledgements
We thank Qihua He (Peking University) for technical assistance with FCCS; Shufeng Sun (the Institute of Biophysics, CAS) for help with TEM; and Jian Xu (National University of Singapore) for kindly providing PIN1-GFP plasmid and *DR5::GFP* seeds.

Funding
This work was supported by the National Basic Research Program of China [2011CB809103 and 2011CB944601], by a project Program for Creative Research Teams [31121065] and by grants from the National Natural Science Foundation of China [30821007 and 31270224].

Competing interests statement
The authors declare no competing financial interests.

Author contributions
L.F. performed experiments, analyzed the data and wrote the manuscript. H.H. performed experiments and analyzed the data. Y.X., L.Z. and K.S. performed experiments. Z.D., M.A.B. and H.W. analyzed the data and assisted in critical revising of the manuscript. J.L. designed the experiment and wrote the manuscript.

Supplementary material
Supplementary material available online at
http://dev.biologists.org/lookup/suppl/doi:10.1242/dev.095711/-/DC1

References
Abrami, L., Bischofberger, M., Kunz, B., Groux, R. and van der Goot, F. G. (2010). Endocytosis of the anthrax toxin is mediated by clathrin, actin and unconventional adaptors. *PLoS Pathog.* **6**, e1000792.
Bacia, K., Kim, S. A. and Schwille, P. (2006). Fluorescence cross-correlation spectroscopy in living cells. *Nat. Methods* **3**, 83-89.
Banbury, D. N., Oakley, J. D., Sessions, R. B. and Banting, G. (2003). Tyrphostin A23 inhibits internalization of the transferrin receptor by perturbing the interaction between tyrosine motifs and the medium chain subunit of the AP-2 adaptor complex. *J. Biol. Chem.* **278**, 12022-12028.
Bar, M., Sharfman, M., Schuster, S. and Avni, A. (2009). The coiled-coil domain of EHD2 mediates inhibition of LeEix2 endocytosis and signaling. *PLoS ONE* **4**, e7973.
Barth, M. and Holstein, S. E. (2004). Identification and functional characterization of *Arabidopsis* AP180, a binding partner of plant alphaC-adaptin. *J. Cell Sci.* **117**, 2051-2062.
Bassham, D. C., Brandizzi, F., Otegui, M. S. and Sanderfoot, A. A. (2008). The secretory system of Arabidopsis. *Arabidopsis Book* **6**, e0116.
Boettner, D. R., Chi, R. J. and Lemmon, S. K. (2012). Lessons from yeast for clathrin-mediated endocytosis. *Nat. Cell Biol.* **14**, 2-10.
Boucrot, E., Saffarian, S., Zhang, R. and Kirchhausen, T. (2010). Roles of AP-2 in clathrin-mediated endocytosis. *PLoS ONE* **5**, e10597.
Chen, C. and Zhuang, X. (2008). Epsin 1 is a cargo-specific adaptor for the clathrin-mediated endocytosis of the influenza virus. *Proc. Natl. Acad. Sci. USA* **105**, 11790-11795.
Chen, X., Irani, N. G. and Friml, J. (2011). Clathrin-mediated endocytosis: the gateway into plant cells. *Curr. Opin. Plant Biol.* **14**, 674-682.
Collins, B. M., McCoy, A. J., Kent, H. M., Evans, P. R. and Owen, D. J. (2002). Molecular architecture and functional model of the endocytic AP2 complex. *Cell* **109**, 523-535.
Conner, S. D. and Schmid, S. L. (2003). Regulated portals of entry into the cell. *Nature* **422**, 37-44.

Cureton, D. K., Massol, R. H., Saffarian, S., Kirchhausen, T. L. and Whelan, S. P. (2009). Vesicular stomatitis virus enters cells through vesicles incompletely coated with clathrin that depend upon actin for internalization. *PLoS Pathog.* **5**, e1000394.
Dhonukshe, P., Aniento, F., Hwang, I., Robinson, D. G., Mravec, J., Stierhof, Y. D. and Friml, J. (2007). Clathrin-mediated constitutive endocytosis of PIN auxin efflux carriers in *Arabidopsis*. *Curr. Biol.* **17**, 520-527.
Dhonukshe, P., Tanaka, H., Goh, T., Ebine, K., Mähönen, A. P., Prasad, K., Blilou, I., Geldner, N., Xu, J., Uemura, T. et al. (2008). Generation of cell polarity in plants links endocytosis, auxin distribution and cell fate decisions. *Nature* **456**, 962-966.
Diril, M. K., Schmidt, S., Krauss, M., Gawlik, V., Joost, H. G., Schürmann, A., Haucke, V. and Augustin, R. (2009). Lysosomal localization of GLUT8 in the testis – the EXXXLL motif of GLUT8 is sufficient for its intracellular sorting via AP1- and AP2-mediated interaction. *FEBS J.* **276**, 3729-3743.
Doherty, G. J. and McMahon, H. T. (2009). Mechanisms of endocytosis. *Annu. Rev. Biochem.* **78**, 857-902.
Doray, B., Lee, I., Knisely, J., Bu, G. and Kornfeld, S. (2007). The gamma/sigma1 and alpha/sigma2 hemicomplexes of clathrin adaptors AP-1 and AP-2 harbor the dileucine recognition site. *Mol. Biol. Cell* **18**, 1887-1896.
Ehrhardt, D. W. and Frommer, W. B. (2012). New technologies for 21st century plant science. *Plant Cell* **24**, 374-394.
Erdel, F., Schubert, T., Marth, C., Längst, G. and Rippe, K. (2010). Human ISWI chromatin-remodeling complexes sample nucleosomes via transient binding reactions and become immobilized at active sites. *Proc. Natl. Acad. Sci. USA* **107**, 19873-19878.
Feraru, E., Paciorek, T., Feraru, M. I., Zwiewka, M., De Groodt, R., De Rycke, R., Kleine-Vehn, J. and Friml, J. (2010). The AP-3 β adaptin mediates the biogenesis and function of lytic vacuoles in Arabidopsis. *Plant Cell* **22**, 2812-2824.
Fitzpatrick, J. A. J. and Lillemeier, B. F. (2011). Fluorescence correlation spectroscopy: linking molecular dynamics to biological function in vitro and in situ. *Curr. Opin. Struct. Biol.* **21**, 650-660.
Fujimoto, M., Arimura, S., Ueda, T., Takanashi, H., Hayashi, Y., Nakano, A. and Tsutsumi, N. (2010). Arabidopsis dynamin-related proteins DRP2B and DRP1A participate together in clathrin-coated vesicle formation during endocytosis. *Proc. Natl. Acad. Sci. USA* **107**, 6094-6099.
Furutani, M., Vernoux, T., Traas, J., Kato, T., Tasaka, M. and Aida, M. (2004). PIN-FORMED1 and PINOID regulate boundary formation and cotyledon development in Arabidopsis embryogenesis. *Development* **131**, 5021-5030.
Happel, N., Höning, S., Neuhaus, J. M., Paris, N., Robinson, D. G. and Holstein, S. E. (2004). Arabidopsis mu A-adaptin interacts with the tyrosine motif of the vacuolar sorting receptor VSR-PS1. *Plant J.* **37**, 678-693.
Hirst, J., Barlow, L. D., Francisco, G. C., Sahlender, D. A., Seaman, M. N., Dacks, J. B. and Robinson, M. S. (2011). The fifth adaptor protein complex. *PLoS Biol.* **9**, e1001170.
Hirst, J., Irving, C. and Borner, G. H. (2013). Adaptor protein complexes AP-4 and AP-5: new players in endosomal trafficking and progressive spastic paraplegia. *Traffic* **14**, 153-164.
Huang, F., Khvorova, A., Marshall, W. and Sorkin, A. (2004). Analysis of clathrin-mediated endocytosis of epidermal growth factor receptor by RNA interference. *J. Biol. Chem.* **279**, 16657-16661.
Jackson, L. P., Kelly, B. T., McCoy, A. J., Gaffry, T., James, L. C., Collins, B. M., Höning, S., Evans, P. R. and Owen, D. J. (2010). A large-scale conformational change couples membrane recruitment to cargo binding in the AP2 clathrin adaptor complex. *Cell* **141**, 1220-1229.
Jaqaman, K., Loerke, D., Mettlen, M., Kuwata, H., Grinstein, S., Schmid, S. L. and Danuser, G. (2008). Robust single-particle tracking in live-cell time-lapse sequences. *Nat. Methods* **5**, 695-702.
Kaiserli, E., Sullivan, S., Jones, M. A., Feeney, K. A. and Christie, J. M. (2009). Domain swapping to assess the mechanistic basis of Arabidopsis phototropin 1 receptor kinase activation and endocytosis by blue light. *Plant Cell* **21**, 3226-3244.
Kelly, B. T. and Owen, D. J. (2011). Endocytic sorting of transmembrane protein cargo. *Curr. Opin. Cell Biol.* **23**, 404-412.
Kelly, B. T., McCoy, A. J., Späte, K., Miller, S. E., Evans, P. R., Höning, S. and Owen, D. J. (2008). A structural explanation for the binding of endocytic dileucine motifs by the AP2 complex. *Nature* **456**, 976-979.
Konopka, C. A., Backues, S. K. and Bednarek, S. Y. (2008). Dynamics of Arabidopsis dynamin-related protein 1C and a clathrin light chain at the plasma membrane. *Plant Cell* **20**, 1363-1380.
Leborgne-Castel, N., Lherminier, J., Der, C., Fromentin, J., Houot, V. and Simon-Plas, F. (2008). The plant defense elicitor cryptogein stimulates clathrin-mediated endocytosis correlated with reactive oxygen species production in bright yellow-2 tobacco cells. *Plant Physiol.* **146**, 1255-1266.
Li, M., Tanaka, Y., Alioua, A., Wu, Y., Lu, R., Kundu, P., Sanchez-Pastor, E., Marijic, J., Stefani, E. and Toro, L. (2010). Thromboxane A2 receptor and MaxiK-channel intimate interaction supports channel trans-inhibition independent of G-protein activation. *Proc. Natl. Acad. Sci. USA* **107**, 19096-19101.
Li, X., Wang, X., Yang, Y., Li, R., He, Q., Fang, X., Luu, D. T., Maurel, C. and Lin, J. (2011). Single-molecule analysis of PIP2;1 dynamics and partitioning reveals multiple modes of Arabidopsis plasma membrane aquaporin regulation. *Plant Cell* **23**, 3780-3797.
Luft, J. H. (1961). Improvements in epoxy resin embedding methods. *J. Biophys. Biochem. Cytol.* **9**, 409-414.
Maldonado-Báez, L. and Wendland, B. (2006). Endocytic adaptors: recruiters, coordinators and regulators. *Trends Cell Biol.* **16**, 505-513.
Mattheyses, A. L., Simon, S. M. and Rappoport, J. Z. (2010). Imaging with total internal reflection fluorescence microscopy for the cell biologist. *J. Cell Sci.* **123**, 3621-3628.
Mattsson, J., Ckurshumova, W. and Berleth, T. (2003). Auxin signaling in Arabidopsis leaf vascular development. *Plant Physiol.* **131**, 1327-1339.
McMahon, H. T. and Boucrot, E. (2011). Molecular mechanism and physiological functions of clathrin-mediated endocytosis. *Nat. Rev. Mol. Cell Biol.* **12**, 517-533.
Men, S., Boutté, Y., Ikeda, Y., Li, X., Palme, K., Stierhof, Y. D., Hartmann, M. A., Moritz, T. and Grebe, M. (2008). Sterol-dependent endocytosis mediates post-cytokinetic acquisition of PIN2 auxin efflux carrier polarity. *Nat. Cell Biol.* **10**, 237-244.
Mettlen, M., Stoeber, M., Loerke, D., Antonescu, C. N., Danuser, G. and Schmid, S. L. (2009). Endocytic accessory proteins are functionally distinguished by their differential effects on the maturation of clathrin-coated pits. *Mol. Biol. Cell* **20**, 3251-3260.
Mitsunari, T., Nakatsu, F., Shioda, N., Love, P. E., Grinberg, A., Bonifacino, J. S. and Ohno, H. (2005). Clathrin adaptor AP-2 is essential for early embryonal development. *Mol. Cell. Biol.* **25**, 9318-9323.
Motley, A., Bright, N. A., Seaman, M. N. and Robinson, M. S. (2003). Clathrin-mediated endocytosis in AP-2-depleted cells. *J. Cell Biol.* **162**, 909-918.
Murashige, T. and Skoog, F. (1962). A revised medium for rapid growth and bio assays with tobacco tissue cultures. *Physiol. Plant* **15**, 473-497.
Naramoto, S., Kleine-Vehn, J., Robert, S., Fujimoto, M., Dainobu, T., Paciorek, T., Ueda, T., Nakano, A., Van Montagu, M. C., Fukuda, H. et al. (2010). ADP-ribosylation factor machinery mediates endocytosis in plant cells. *Proc. Natl. Acad. Sci. USA* **107**, 21890-21895.
Owen, D. J., Collins, B. M. and Evans, P. R. (2004). Adaptors for clathrin coats: structure and function. *Annu. Rev. Cell Dev. Biol.* **20**, 153-191.
Pan, J., Fujioka, S., Peng, J., Chen, J., Li, G. and Chen, R. (2009). The E3 ubiquitin ligase SCFTIR1/AFB and membrane sterols play key roles in auxin regulation of endocytosis, recycling, and plasma membrane accumulation of the auxin efflux transporter PIN2 in Arabidopsis thaliana. *Plant Cell* **21**, 568-580.
Péret, B., Swarup, K., Ferguson, A., Seth, M., Yang, Y., Dhondt, S., James, N., Casimiro, I., Perry, P., Syed, A. et al. (2012). AUX/LAX genes encode a family of auxin influx transporters that perform distinct functions during Arabidopsis development. *Plant Cell* **24**, 2874-2885.
Pérez-Gómez, J. and Moore, I. (2007). Plant endocytosis: it is clathrin after all. *Curr. Biol.* **17**, R217-R219.
Robinson, M. S. (1987). 100-kD coated vesicle proteins: molecular heterogeneity and intracellular distribution studied with monoclonal antibodies. *J. Cell Biol.* **104**, 887-895.
Robinson, M. S. (2004). Adaptable adaptors for coated vesicles. *Trends Cell Biol.* **14**, 167-174.
Samaj, J., Read, N. D., Volkmann, D., Menzel, D. and Baluska, F. (2005). The endocytic network in plants. *Trends Cell Biol.* **15**, 425-433.
Schmid, E. M. and McMahon, H. T. (2007). Integrating molecular and network biology to decode endocytosis. *Nature* **448**, 883-888.
Serino, G. and Deng, X.W. (2007). Protein coimmunoprecipitation in Arabidopsis. *CSH Protocols* **2007**, pdb prot4683.
Sorkin, A. and von Zastrow, M. (2009). Endocytosis and signalling: intertwining molecular networks. *Nat. Rev. Mol. Cell Biol.* **10**, 609-622.
Taylor, M. J., Perrais, D. and Merrifield, C. J. (2011). A high precision survey of the molecular dynamics of mammalian clathrin-mediated endocytosis. *PLoS Biol.* **9**, e1000604.
Traub, L. M. (2009). Tickets to ride: selecting cargo for clathrin-regulated internalization. *Nat. Rev. Mol. Cell Biol.* **10**, 583-596.
Wan, Y., Ash, W. M., III, Fan, L., Hao, H., Kim, M. K. and Lin, J. (2011). Variable-angle total internal reflection fluorescence microscopy of intact cells of Arabidopsis thaliana. *Plant Methods* **7**, 27.
Yeung, B. G., Phan, H. L. and Payne, G. S. (1999). Adaptor complex-independent clathrin function in yeast. *Mol. Biol. Cell* **10**, 3643-3659.
Yu, A., Rual, J. F., Tamai, K., Harada, Y., Vidal, M., He, X. and Kirchhausen, T. (2007). Association of Dishevelled with the clathrin AP-2 adaptor is required for Frizzled endocytosis and planar cell polarity signaling. *Dev. Cell* **12**, 129-141.
Zimmermann, P., Hirsch-Hoffmann, M., Hennig, L. and Gruissem, W. (2004). GENEVESTIGATOR. Arabidopsis microarray database and analysis toolbox. *Plant Physiol.* **136**, 2621-2632.
Zinchuk, V., Wu, Y., Grossenbacher-Zinchuk, O. and Stefani, E. (2011). Quantifying spatial correlations of fluorescent markers using enhanced background reduction with protein proximity index and correlation coefficient estimations. *Nat. Protoc.* **6**, 1554-1567.
Zwiewka, M., Feraru, E., Möller, B., Hwang, I., Feraru, M. I., Kleine-Vehn, J., Weijers, D. and Friml, J. (2011). The AP-3 adaptor complex is required for vacuolar function in Arabidopsis. *Cell Res.* **21**, 1711-1722.

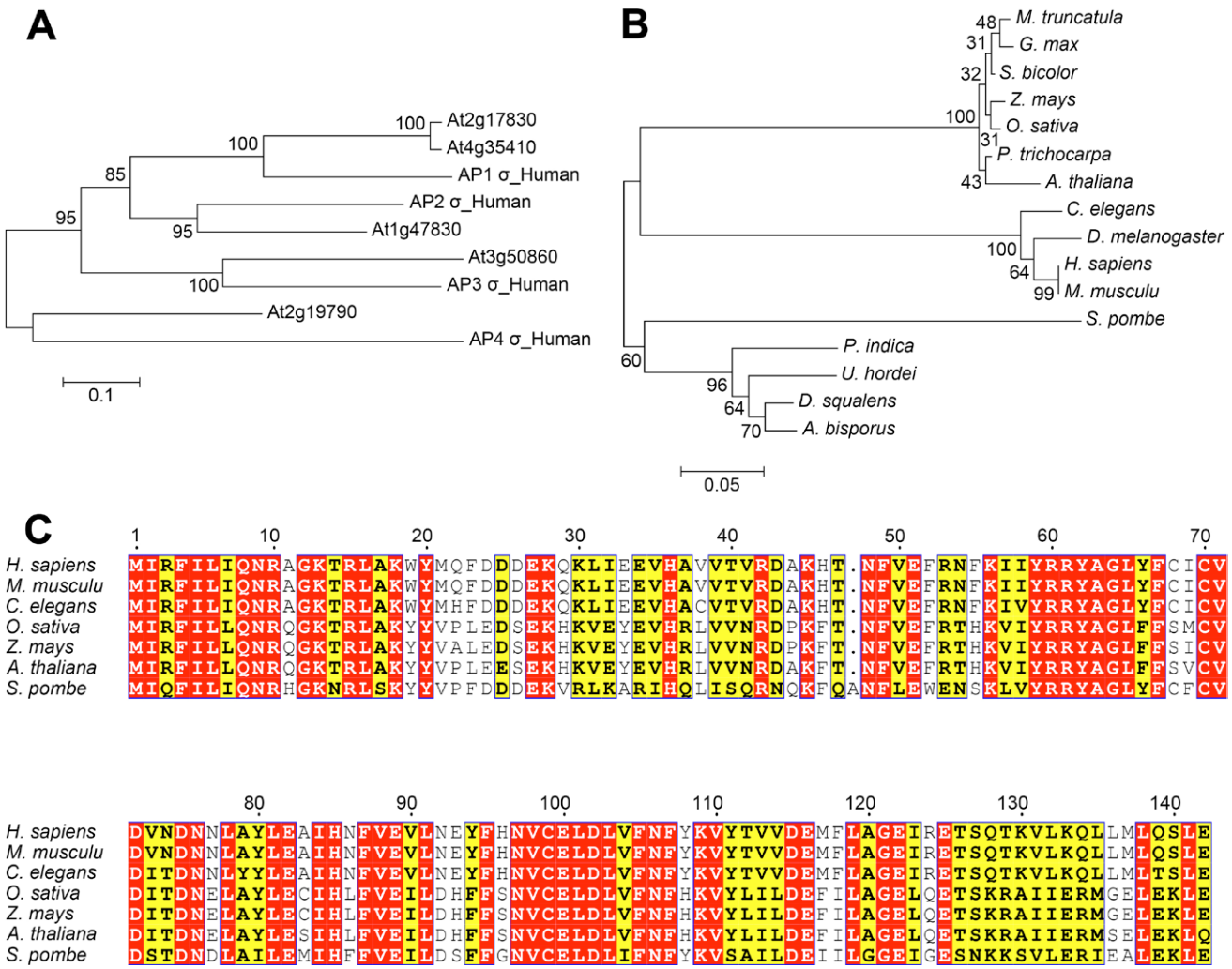

Fig. S1. Phylogenetic analysis of putative AP2 σ in plants, animals and fungi. (**A**) Phylogenetic analysis of putative σ subunits in AP1, AP2, AP3 and AP4 from *Arabidopsis* and human. The aligned sequences were used to construct a phylogenetic tree using MEGA4. Bootstrap values are shown in percentages at the branch nodes. (**B**) Phylogenetic analysis of AP2 σ from a range of eukaryotic organisms. (**C**) Sequence alignment of AP2 σ homologs from different species. The alignment was generated using ClustalW and Espript (http://espript.ibcp.fr/ESPript/ESPript/).

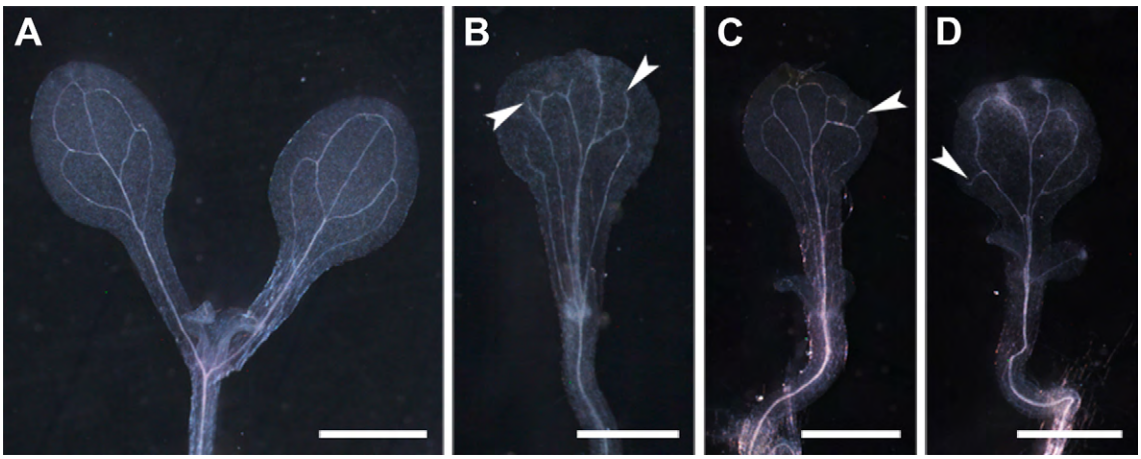

Fig. S2. Vascular patterns in the *ap2 σ* mutant. Vascular patterns of the cotyledon of 7-day-old seedlings in (**A**) the wild type and (**B-D**) the *ap2 σ* mutant. Note that the *ap2 σ* mutant shows various abnormal vascular patterns. Scale bars: 1 mm.

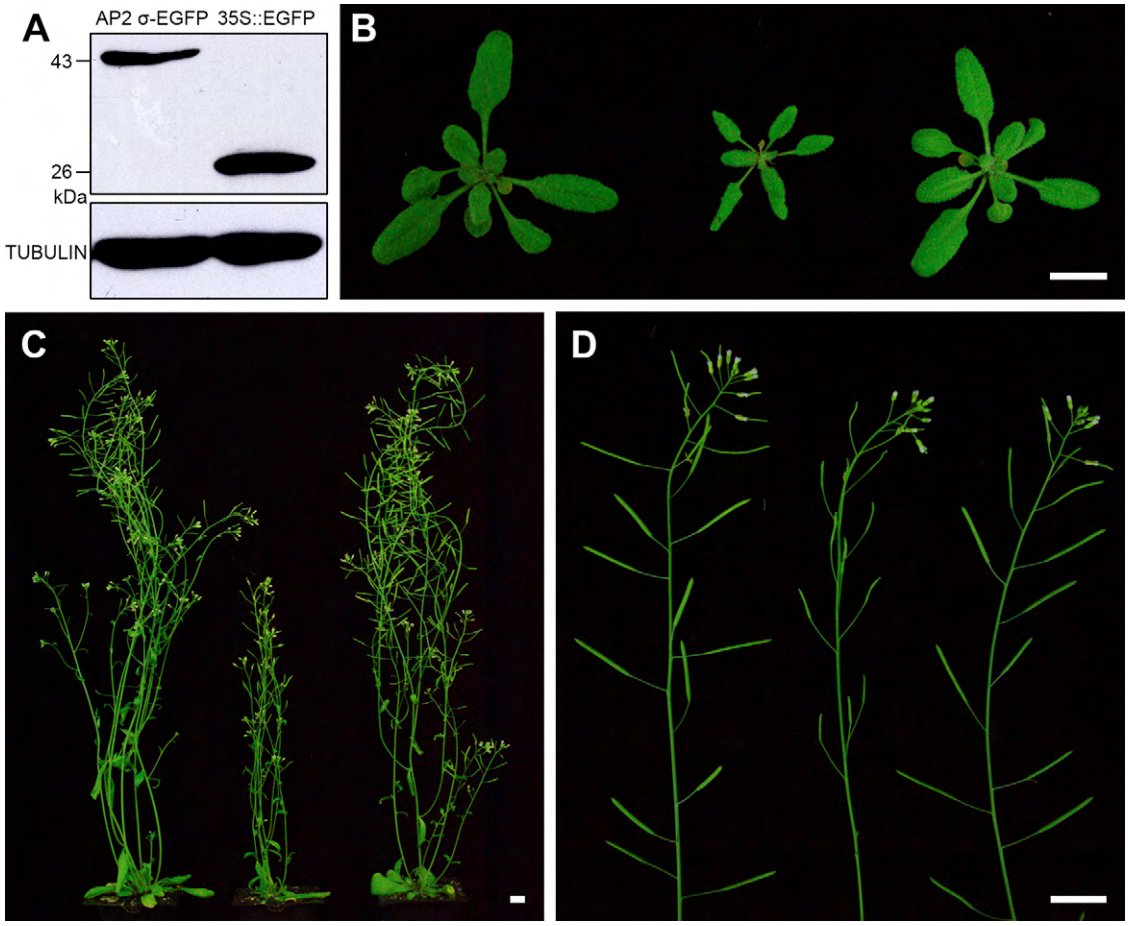

Fig. S3. Rescue of the *ap2 σ* mutant by an *AP2 σ-EGFP* genomic sequence. (**A**) Immunoblot analysis of total protein extracts from 10-day-old *AP2 σ-EGFP* and *35S::EGFP* (as a control) transgenic *Arabidopsis* seedlings probed with GFP antibody. (**B**,**C**) Three-week-old and 6-week-old seedlings of wild-type (left), *ap2 σ* mutant (middle) and *AP2 σ-EGFP genomic*; *ap2 σ* complementary plants (right). (**D**) Inflorescences of wild-type, *ap2 σ* and *AP2 σ-EGFP genomic*; *ap2 σ* complementary plants showing that the complementary plants have a normal silique length. Scale bars: 10 mm.

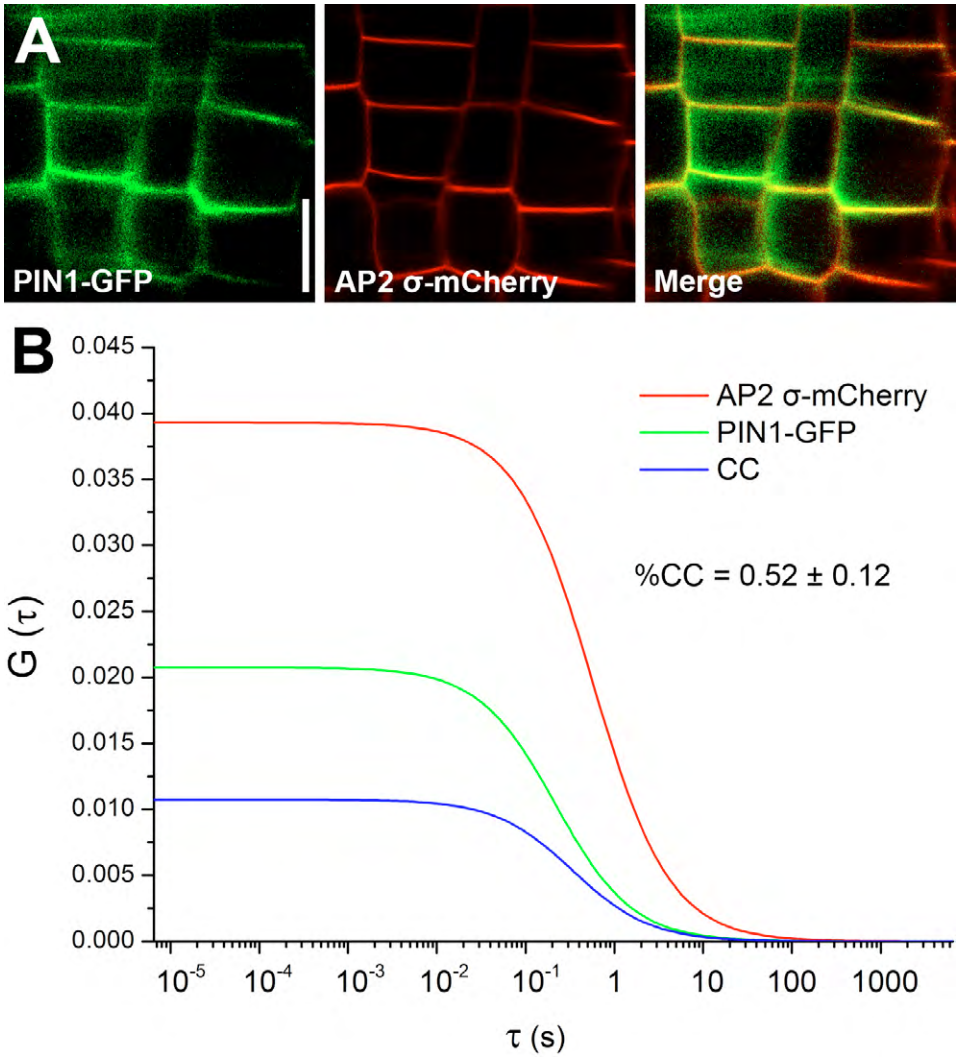

Fig. S4. Colocalization and FCCS analysis of PIN1-GFP and AP2 σ-mCherry in living cells. (**A**) Confocal microscopy images of living cells expressing PIN1-GFP and AP2 σ-mCherry. (**B**) FCCS analysis of the cross-correlation of PIN1-GFP and AP2 σ-mCherry. Note that PIN1-GFP colocalized remarkably with AP2 σ-mCherry. The cross-correlation value was 0.52±0.12 for PIN1-GFP to AP2 σ-mCherry. Scale bar: 10 μm.

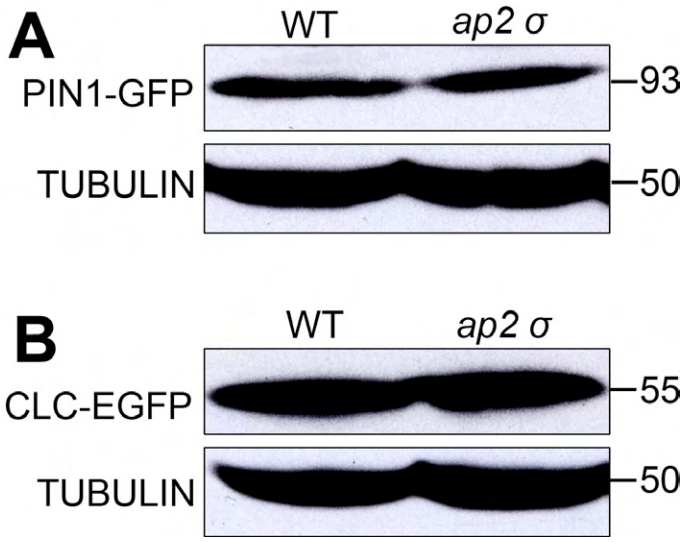

Fig. S5. Immunoblot analysis of PIN1-GFP and CLC-EGFP protein levels in wild type and *ap2 σ* mutant. PIN1-GFP (**A**) and CLC-EGFP (**B**) samples were probed with anti-GFP antibody and TUBULIN was used as a loading control. Note that CLC-EGFP and PIN1-GFP showed similar expression levels in the wild type and *ap2 σ* mutant.

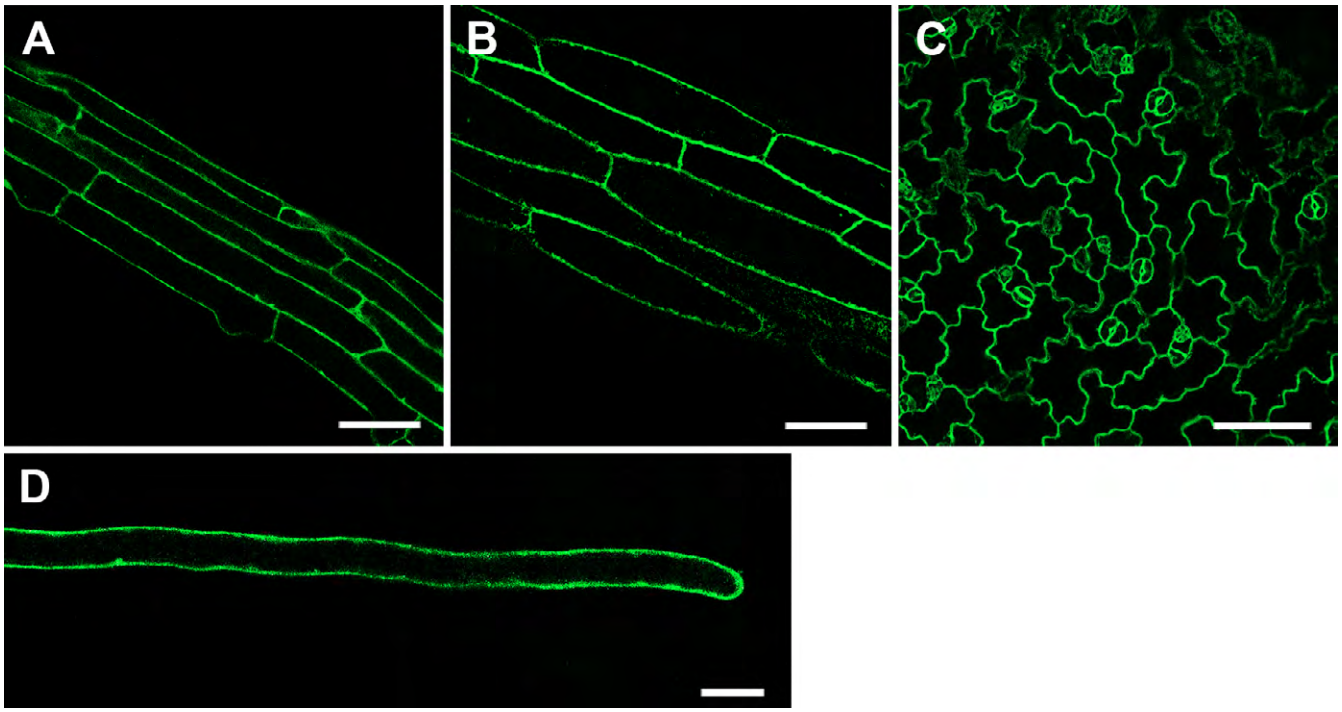

Fig. S6. Subcellular localization of AP2 σ-EGFP. Confocal microscopy images of AP2 σ-EGFP showing (**A**) root epidermal cells, (**B**) hypocotyl epidermal cells, (**C**) leaf pavement cells and (**D**) growing root hair. Scale bars: 50 μm in A-C; 10 μm in D.

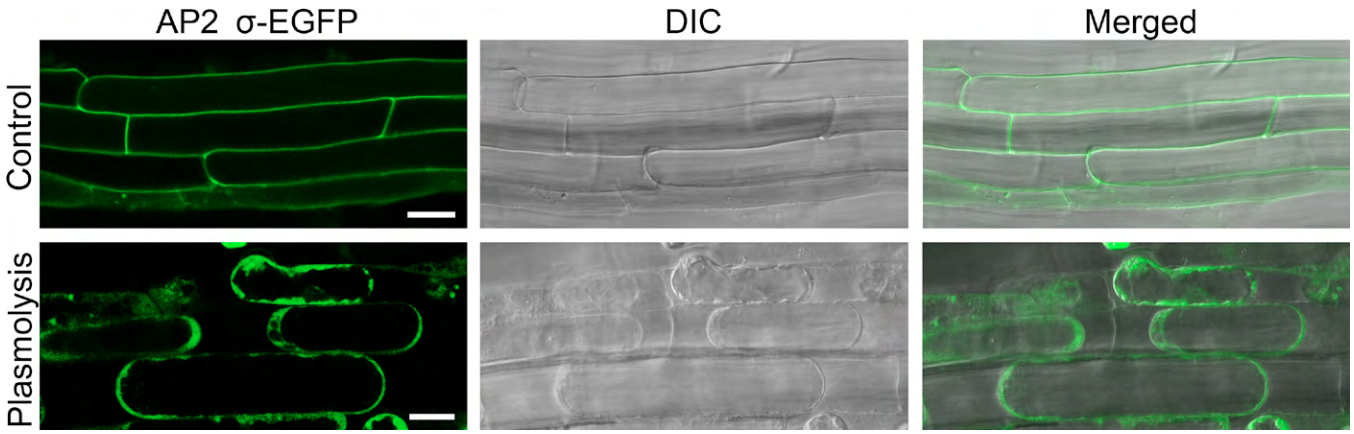

Fig. S7. NaCl-induced plasmolysis. Roots were plasmolyzed by treatment with 1 M NaCl for 5 minutes, showing that AP2 σ-EGFP is localized at the plasma membrane and the cytoplasm. Scale bars: 20 μm.

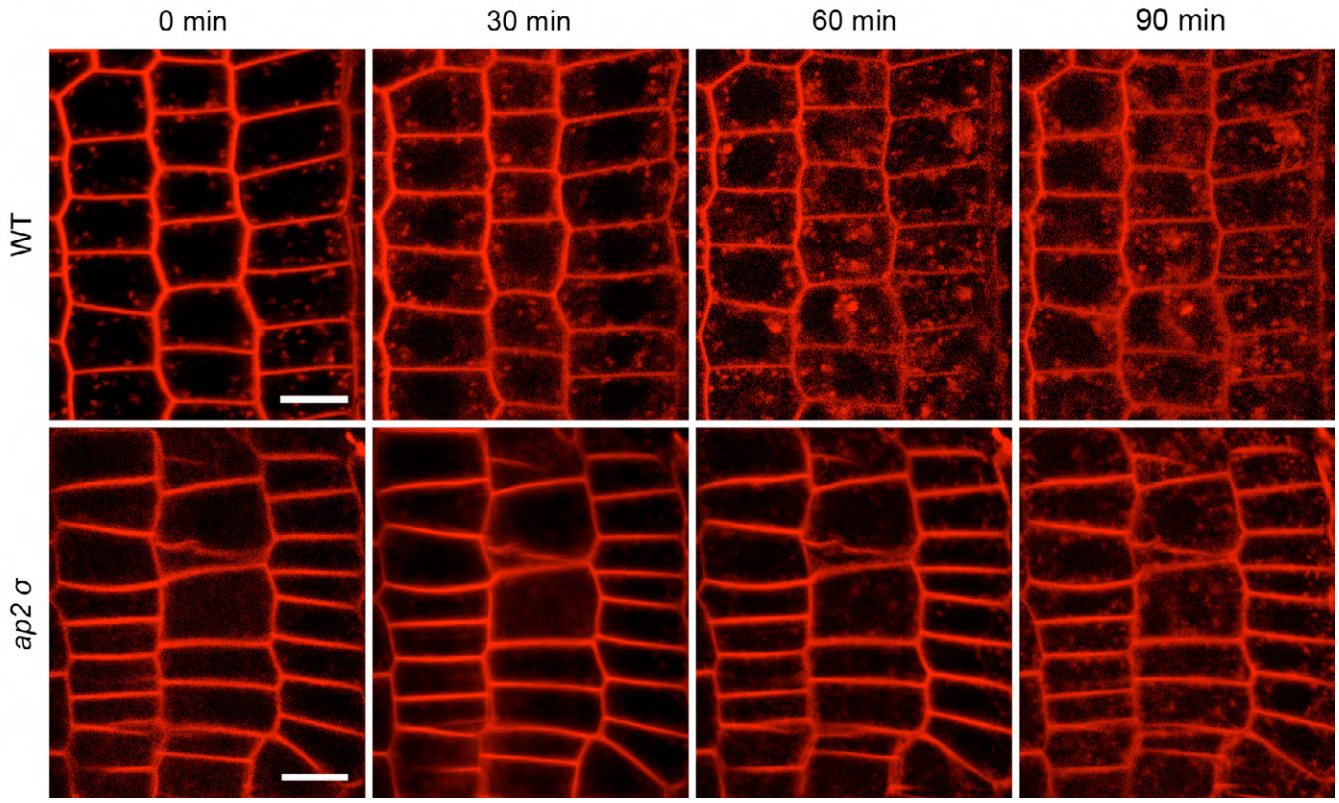

Fig. S8. Monitoring the uptake of FM4-64 on a long time scale in the wild type and *ap2 σ* mutant. Seedling roots of the wild type and *ap2 σ* mutant were pulse labeled with FM4-64 and monitored for 90 minutes at 30-minute intervals. Note that *ap2 σ* only showed a small amount of internalization of FM4-64 90 minutes after labeling. Scale bar: 10 μm.

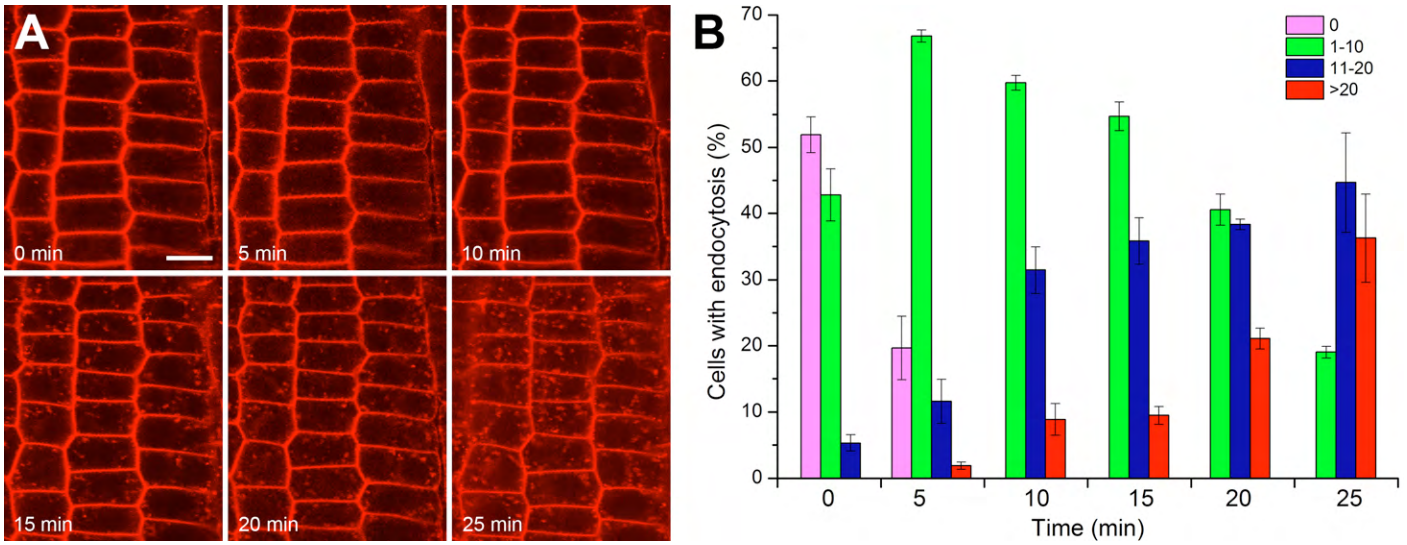

Fig. S9. Analysis of endocytic rate in the complementation line of *ap2 σ*. (**A**) Timecourse of FM4-64 internalization in the complementation line of *ap2 σ*. (**B**) Quantitative analysis of the endocytic rate in the complementation line of *ap2 σ*. Scale bar: 10 μm.

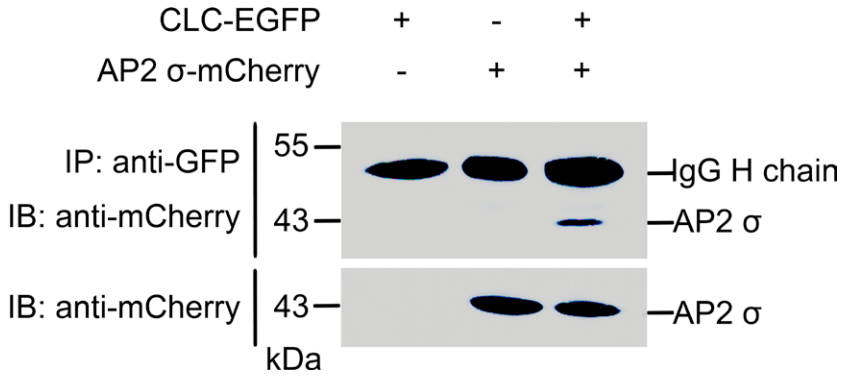

Fig. S10. Co-immunoprecipitation of CLC with AP2 σ in transgenic *Arabidopsis*. Total protein extracts from CLC-EGFP, AP2 σ-mCherry and CLC-EGFP/AP2 σ-mCherry transgenic plants were immunoprecipitated (IP) with anti-GFP. IP proteins (upper panel) and input (lower panel) were detected by immunoblot (IB) with anti-mCherry antibody.

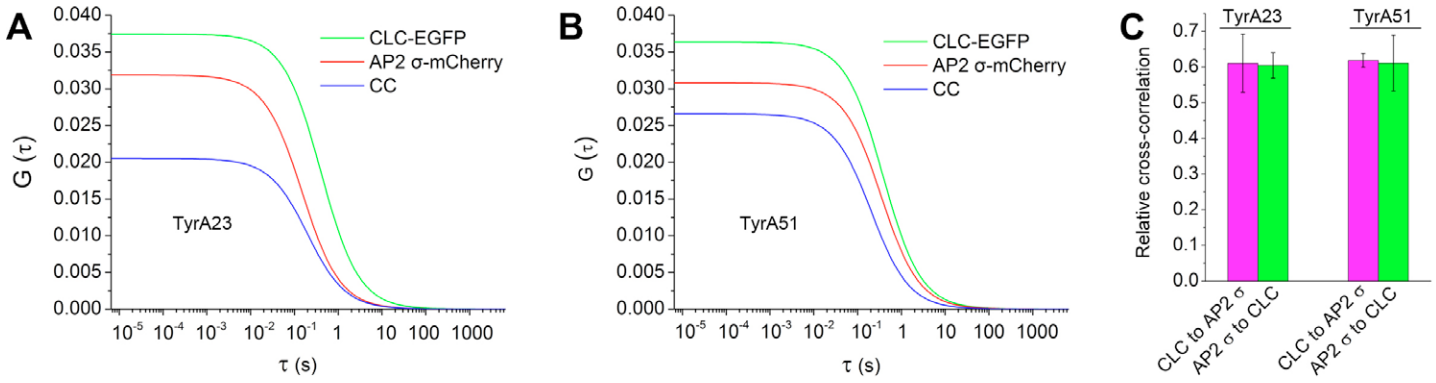

Fig. S11. FCCS analysis of the association of CLC-EGFP and AP2 σ-mCherry after TyrA23 and TyrA51 treatment. (**A**,**B**) The autocorrelation and cross-correlation curves from FCCS experiments. (A) TyrA23 treatment, (B) TyrA51 treatment. (**C**) Cross-correlation value between CLC-EGFP and AP2 σ-mCherry after treatment with TyrA23 and TyrA51. Note that neither TyrA23 nor TyrA51 had any significant effects on the association between CLC-EGFP and AP2 σ-mCherry. *n*=40 measurements from 10 roots. Student's *t*-test, $P<0.01$.

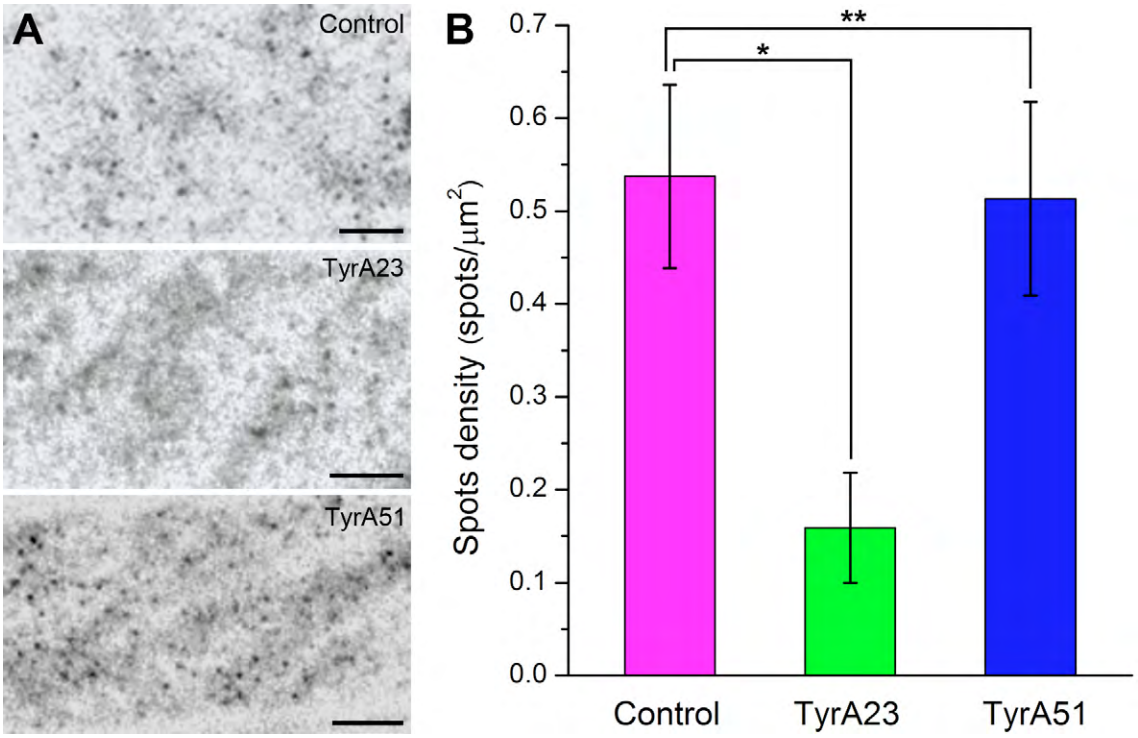

Fig. S12. Effects of TyrA23 on the localization of AP2 σ on the plasma membrane. (**A**) VA-TIRFM image of AP2 σ-EGFP in control cells (top panel), and epidermal cells treated with TyrA23 (middle) or TyrA51 (bottom). (**B**) Densities of AP2 σ-EGFP spots in control, TyrA23- and TyrA51-treated cells. *n*=10 roots. Student's *t*-test, **P*<0.01, ***P*>0.5. Scale bars: 5 μm.

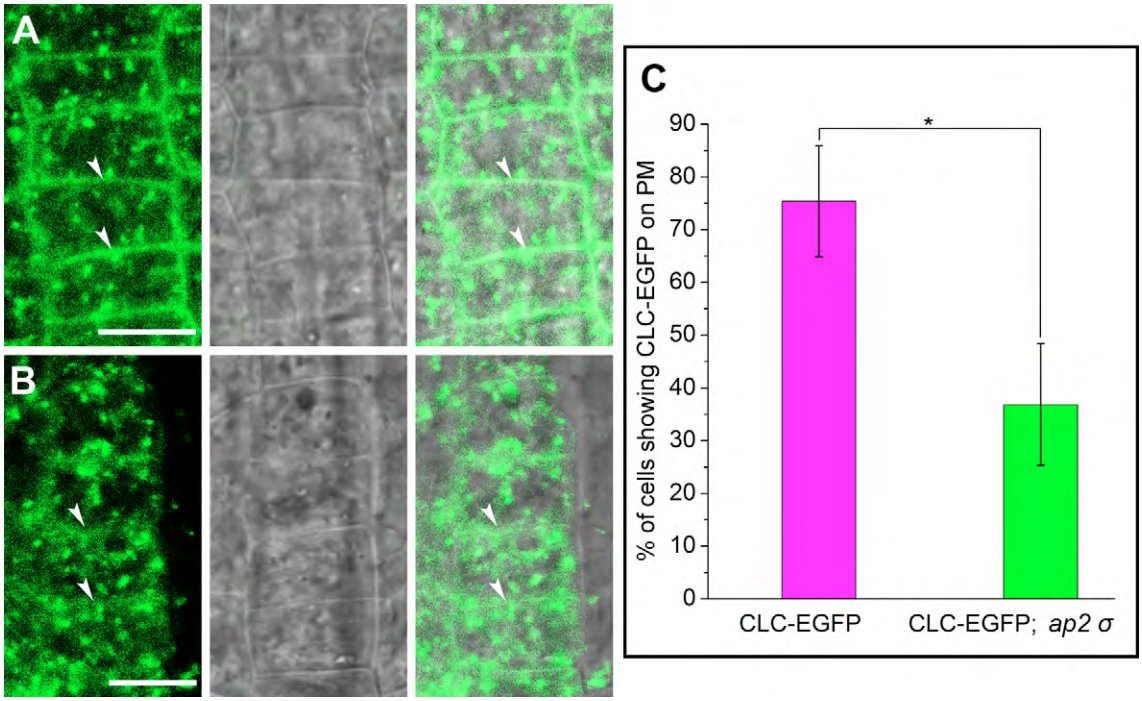

Fig. S13. Subcellular localization of CLC-EGFP in the *ap2 σ* mutant. (**A**,**B**) Localization of clathrin as visualized by CLC-EGFP in the wild type (A) and *ap2 σ* mutant (B). (**C**) Measurement of the percentage of PM-localized clathrin-containing cells in the wild type and *ap2 σ* mutant. Note that in the *ap2 σ* mutant CLC-EGFP remained localized in the cytoplasm but deceased at the plasma membrane (PM). *n*=10 roots; Student's *t*-test, **P*<0.01. Scale bars: 10 μm.

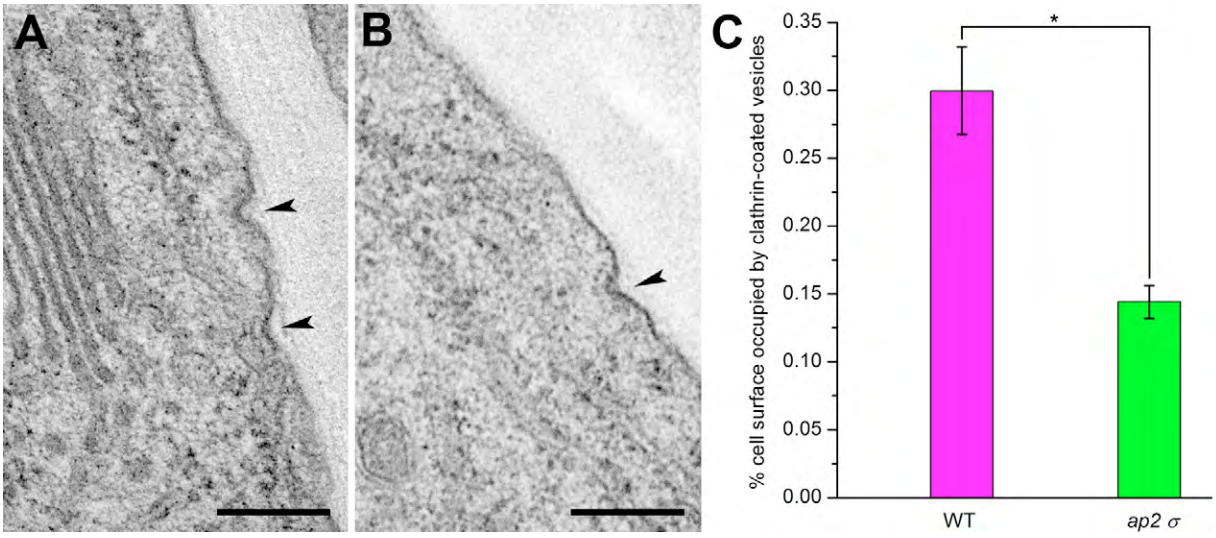

Fig. S14. TEM analysis of clathrin-coated vesicles on the plasma membrane. (**A**,**B**) Electron micrograph of clathrin-coated vesicles in the wild type (A) and *ap2 σ* mutant (B). (**C**) Percentage of the cell surface occupied by clathrin-coated vesicles in the wild type and *ap2 σ* mutant. *n*=40 sections from three embedded blocks. Student's *t*-test, **P*<0.01. Scale bars: 200 nm.

Movie 1. Dynamic behavior of AP2 σ-EGFP at the plasma membrane of *Arabidopsis* root epidermal cells. The movie consists of 100 VA-TIRFM images acquired at 1-second intervals.

Movie 2. Dynamic behavior of CLC-EGFP at the plasma membrane of *Arabidopsis* root epidermal cells. The movie consists of 100 VA-TIRFM images acquired at 1-second intervals.

Movie 3. Dynamic behavior of CLC-EGFP at the plasma membrane of *Arabidopsis* root epidermal cells in the *ap2 σ* mutant. The movie consists of 100 VA-TIRFM images acquired at 1-second intervals.

Table S1. The frequency of abnormal cotyledon phenotypes

Phenotype	*ap2 σ*	Wild type
Normal	102	120
Single cotyledon	14 (11.0%)	0
Trumpet-shaped	8 (6.3%)	0
Triple cotyledons	3 (2.3%)	0

Table S2. FRAP analysis of AP2 σ-EGFP dynamics in growing root hairs

Region	Percentage recovery	$t_{1/2}$ (S)	*n*
Top	73.1±7.6	11.5±5.0	10
Middle	78.1±16.5	10.0±3.1	10
Bottom	73.4±13.6	10.3±2.9	10

Values are mean ± s.d.

Table S3. Primers

Primer	Sequence (5′-3′)
CLC_for	GCGCTGCAGGAGTCGGAGATGATGATTATGATG
CLC_rev	GATACTAGTAGCTCCTCCTCCTCCAGCAGCAGTAACTG CCTCAGTGGGC
mCherry_for	ATGGTACCATGGTGAGCAAGGGCGAGGAGG
mCherry_rev	ATGGATCCCTACTTGTACAGCTCGTCCATGCCG
AP2 σ_for	CGCTGCAGAGGTAAAAGAACCGTTGTGGCTATG
AP2 σ_rev	ATGGTACCAGCTCCTCCTCCTCCCTGTAGCTTCTCGAGT TCTGACATC
LB1.3	ATTTTGCCGATTTCGGAAC
SALK_141555_for	GATATTGGACCATTTCTTCAGC
SALK_141555_rev	TTATCAGTGGAGGACAAAGAAGG
AP2 σ-RT_for	ATCCGATTCATATTATTGCAGAAC
AP2 σ-RT_rev	AACTCAACAAAGTATAGCAAATCTCTG
TUB_for	CGTGGATCACAGCAATACAGAGCC
TUB_rev	CCTCCTGCACTTCCACTTCGTCTTC